2017

Fabricating copper-rich Cu-Al binary alloy by wire-arc additive manufacturing

Bosheng Dong
University of Wollongong

Fabricating copper-rich Cu-Al binary alloy by wire-arc additive manufacturing

Master of philosophy

From

University of Wollongong

by

Bosheng Dong, Bachelor of Engineering

School of Mechanical, Materials and Mechatronic Engineering

Faculty of Engineering and Information Sciences

March, 2017

Declaration

I, Bosheng Dong, declare that this thesis, submitted in fulfillment of the requirements for award of Master of Philosophy, in the School of Mechanical, Materials and Mechatronic Engineering, University of Wollongong, Australia, is wholly my own work unless otherwise referenced or acknowledged. The document has not been submitted for qualifications at any other academic institution.

Bosheng Dong

March, 2017

Table of Contents

List of Figures

Chapter 2:

Chapter 3:

Chapter 4:

Chapter 5:

Chapter 6:

List of Tables

List of Abbreviations and Symbol

1. Abbreviations

AM	additive manufacturing
WAAM	wire-arc additive manufacturing
GTAW	gas tungsten arc welding
GMAW	gas metal arc welding
TIG	tungsten inert gas
SAW	submerged arc welding
SFE	stacking fault energy
3D	three-dimensional
CAD	computer aided design
SEM	scanning electron microscopy
EDS	energy dispersive spectrometer
OM	optical microscopy
XRD	X-ray diffraction
OP-S	oxide polishing suspensions
UTS	ultimate tensile strength
YS	yield strength

2. Symbol

°C	Celsius degree
Q_R	resistance heat
I	welding current

A	amp
R	equivalent resistance of welding arc
t	time
h	hour
min	minute
s	second
η	heat input efficiency
U	welding voltage
V	volt
v	travel speed
°	degree
at.%	atom percent
wt.%	weight percent
mm/s	millimeter per second
mm/min	millimeter per minute
L/min	liter per minute
α	alpha phase
kg/m^3	kilogram per square meter
s^{-1}	per second
λ	wave length
mm	millimeter
μm	micron
Hv	Vickers hardness
MPa	mega Pascal
Å	angstrom

Abstract

In response to the needs of increasing the usability of the wire-arc additive manufacturing process(WAAM) and offering an innovative way of producing Cu-Al alloys with controlled chemical compositions, the present research has applied the WAAM process in Cu-Al alloy with targeted 9 at. % Al content on pure copper plates. After overcoming several processing problems such as opening the deposition molten pool on the extremely high-thermal conductive copper plate and conducting the Al wire into the molten pool with very low feed speed, the copper rich Cu-Al alloy has been successfully produced with constant pre-designed Al content above the dilution affected area. Also, in order to homogenize the as-fabricated material and improve the mechanical properties, two further homogenization heat treatments at 800 °C and 900 °C have been applied. The material and mechanical properties of as-fabricated and heat-treated samples have been compared and analyzed in detail. With increased annealing temperatures, the content of precipitate phases has decreased, and the samples have shown obvious improvements in both strength and ductility with little variation in microstructures. The present research opened a gate for in-situ fabrication of Cu-Al alloy with target chemical composition and full-density using additive manufacturing process.

Keywords: copper alloy, additive manufacturing, mechanical properties, heat treatment

Acknowledgement

My sincere gratitude is to my supervisors Dr. Zengxi Pan and Prof. Huijun Li who gave me this invaluable opportunity to pursue my study as a master student in University of Wollongong (UOW). Also, it should be mentioned that I would like to acknowledge Prof. Zhengyi Jiang and Mr. Yi Yan for the help of using the KTL 1400 tube furnace in their research group during the annealing research. In addition, thanks are due to Dr. Chen Shen, Dr. Yan Ma, Dr. Donghong Ding and Mr. Bintao Tao, my fellow researchers who gave me very meaningful and specific advice about writing this thesis.

Finally, I would like to thank my parents and relatives for their constant support and encouragement during the progression of this thesis.

Chapter 1 Introduction

1.1 Research background

Cu-Al series alloys have continuously been desired for the applications in fossil energy pipelines and certain parts (such as propellers, valves and laminated plates) in shipbuilding industries, due to its outstanding wear and corrosion resistance in highly corrosive environments [1]. As the solid solution element in the Cu-Al alloy, Al element mainly helps to increase the formation of deformation twins and dislocation density during the deformation twinning process [2], which intrinsically refines the grain size and optimizes the mechanical properties, such as hardness and yield strength of the Cu-Al alloy [3]. Researches of the Cu-Al alloy have focused on improving the strength of the material by optimizing the crystal structures to reducing the stacking fault energy inside the material using: micro-alloying elements such as Ni, Zr, Cr and Ag (more references needed) [4]; and plastic deformations such as cold rolling, equal-channel angular pressing and high-pressure torsion.

In recent years, binary Cu-Al alloy in which Al content ranges between 0 at.% to 16.8 at.% (fcc α-phase region) has gained considerable attentions, since the deformation twinning mechanism in these alloys has generated special phenomenon that the ductility of gradient structured Cu-Al first increases then decreases with decreasing stacking fault energy [5-7]. Also, this solid solution α-phase Cu-Al alloy is used as the material to further investigate the relationship between deformation twinning and stacking fault energy [8].

Currently, the Cu-Al alloys are mainly produced using powder metallurgy processes such as laser beam melting [7], arc furnace melting [5] and ball milling [9, 10]. Although powder based technology is capable of fabricating small sized components with good accuracy [11], the metallic powder should be melted or mixed in a sealed chamber with shielding gas or even vacuum, which requires expensive hardware. In addition, these processes lack the flexibility of producing complex geometries and tends to generate defects such as un-melted particles, and micro-cracks. Therefore, an alternative manufacturing process is highly expected for the wider applications of Cu-Al alloys.

In the present work, the Wire-Arc Additive Manufacturing (WAAM) process is adopted to produce target Cu-Al alloy. WAAM system, using either gas tungsten arc welding (GTAW) or gas metal arc welding (GMAW) as heat source, produces components in a layer-by-layer manner. The shielding gas ensure that the sample is isolated with atmospheric air. The protection guarantees the purity of raw material especially for the copper and aluminium which are known as active metal [12].

As a type of rapid prototyping (RP) method, WAAM has gained increasing research interests due to its low material and production cost and its capability of producing very large part with medium complexity [13]. Particularly for the aerospace industry which suffers from high buy-to-fly ratio and has high mechanical quality requirements, the WAAM technology becomes attractive candidate process [14], as it is capable of producing full-density components. Compared to GMAW system, the GTAW system was applied in our work as the power source due to its more stable arc and less inclined

to generate spatter when producing a wide range of non-ferrous alloys and their combinations [15].

To date, the WAAM process has been successfully applied to in-situ fabricate Ti-Al [16] and Fe-Al [17] series alloys with pre-designed chemical compositions and dimensions. And the feasibility of the present process fabricating the target material has been basically proved. However, different from the fabrications of Ti-Al and Fe-Al series alloys, which both have used relatively low thermal conductive pure Ti plate and steel plate as the buildup substrate [18, 19], the fabrication of Cu-Al alloy would have to use copper plate as the substrate, which has extremely high thermal conductivity. It would be significantly difficult to generate the molten pool for the buildup depositions, since the intrinsic high thermal conductivity of copper plate would make it very hard to accumulate enough thermal energy on the certain deposition point and melt the substrate material. Therefore, in addition to the general parameters such as deposition current, voltage and wire feed speed of filler material, the pre-heating temperature, interpass temperature and probably substrate dimensions would significantly influence the qualities of target Cu-Al alloy. In order to understand and mature the WAAM process on Cu-Al alloys, further experimental investigation on the material and mechanical properties of additive manufactured Cu-Al alloy is desired.

1.2 Aims and objectives

The main objectives of the present research subject are:

(i) the feasibility study of manufacturing Cu-Al alloy using WAAM process with

two independent wire feeders to achieve desired chemical composition through controlling the transforming speed of each wire.

The feasibility of WAAM in copper rich Cu-Al alloy fabrication is investigated by fabricating a 15-layer build-up wall by controlling the parameters of deposition processes. The composition and phase characters will be presented to prove the feasibility.

(ii) investigation on the material and mechanical properties of the buildup Cu-Al material

In order to exhibit the properties of Cu-Al alloy fabricated by WAAM system, the microstructure will be observed and hardness test and tensile test were used to show the mechanical properties of welded Cu-Al alloy.

(iii) finding the appropriate heat treatment method to homogenize the material properties of the deposited material.

Considering the segregation in welding process, this work compared the as-fabricated sample with the annealed specimens. The annealing temperature was set at 800°C and 900°C respectively.

1.3 Major contribution

In present research, wire arc additive manufacturing instead of conventional powder metallurgy process is applied to fabricated Cu-Al alloy. The experimental results of the reproducible Cu-Al build-up wall prove the feasibility of WAAM system to fabricate Cu-Al binary alloy with pre-designed chemical compositions. The appropriate parameters for Cu-Al alloy is provided to deposit 15-layer wall. Additionally, by discussing the annealing process, the segregation existing in as-fabricated welded wall is eliminated. Comparing the as-fabricated and annealed sample shows the increase of mechanical properties of Cu-Al buildup wall and the decrease of content of impurity.

Thus, the present study mainly proves that the WAAM process is capable to fabricate Cu-Al alloy with full density which is a necessity for structure materials initially. Secondly, by providing the specific welding parameters, the application of WAAM is also broaden. Finally, homogeneous annealing process is demonstrated for improving the mechanical properties of Cu-Al alloy.

1.4 Thesis outline

This chapter introduces the research background, the research objectives and the contributions of present work. The rest of thesis is divided into 7 section.

In Chapter 2, a literature review shows comprehensive knowledge in current state related to the research subject. Firstly, the design of fabricating system such as the categories of AM processes and the differences between wire feed and powder based are discussed. Secondly, the controlling of WAAM parameters including selection of

power source, arc voltage (arc length), welding current, welding speed and wire-feeding rate is demonstrated. Then, the fundamental knowledge of copper and Cu-Al binary system is exhibited. Ultimately, the influence of heat treatment and generating twin crystal in Cu-Al solid solution is explained.

The experimental setup in present research is exhibited in Chapter 3, which includes the hardware setup, specific welding parameters and the sample preparation process. In addition, the equipment utilized in present study is also presented.

In Chapter 4, the microstructure, macrostructure and phase characterization of as-fabricated sample and annealed sample is illustrated. The typical columnar grain is shown in the deposition wall. The reason why the annealing twin acquired in the top region of annealing sample is explained. Furthermore, the principle of XRD and the XRD testing machine is presented while the transformation of phase after annealing process is demonstrated.

In order to prove the feasibility of WAAM process, Chapter 5 shows the composition of aluminium in build-up wall. The hardness of three type of specimens, as-fabricated sample, annealed at 800°C sample and annealed at 900°C sample are compared at the same time.

Tensile testing is discussed in Chapter 6, which mainly introduce the principle of tension test and the tension testing machine. Subsequently, as-fabricated sample and the sample annealed at 900°C will be compared in the tensile testing result including tensile strength (UTS), 0.2% offset yield strength (0.2%YS) and the elongation and the

morphology of fracture surface.

Chapter 7 shows the primary findings of this wok and makes recommendations for the future work of Cu-Al research.

Chapter 2 Literature Review

2.1 Process design

Copper rich Cu-Al alloys have drawn great attention because of its excellent physical and chemical properties, good corrosion resistance and low material cost [20]. Based on that, aluminium bronze is widely utilized in the general sea water-related service, water supply, oil and petrochemical industries, specialized anti-corrosive applications and certain structural retrofit building applications [21]. In previous works, researchers mainly focused on studying the special properties of Cu-Al solid solution with low stacking faults energy, especially the creep phenomenon [22], cyclic hardening behavior [23], stress corrosion cracking of twist boundary [24] and deformation mechanism [25]. Moreover, in the mentioned researches, the content of aluminium which is lower than 16 at. % gained more interests. According to the Cu-Al equilibrium diagram, while the content of Al is lower than 16 at. %, homogeneous alloys structure is created by α solid solution crystals with body centered cubic lattice. Casting and powder metallurgy such as vacuum melting was used to produce Cu-Al sample. However, as the high oxidability of both copper and aluminium, conventional casting of Cu-Al alloys is inapplicability. In terms of powder metallurgy, expensive processes such as hot isostatic pressing to achieving full density and vacuum chamber for electron beam are required. Thus, innovating low cost manufacturing method for Cu-Al alloy is the future research area.

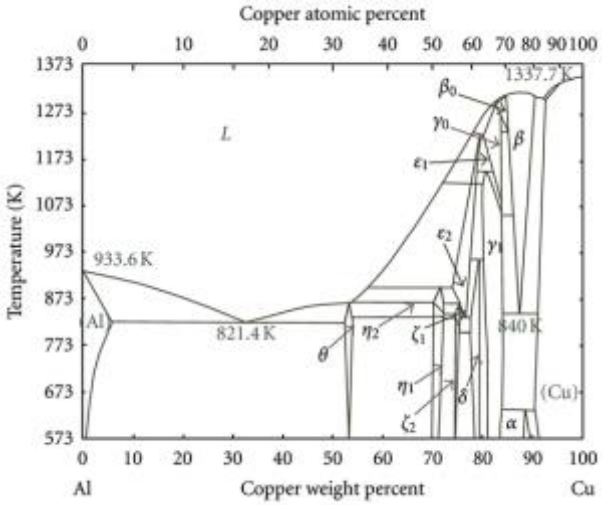

Figure 2. 1 Cu-Al system equilibrium phase diagram [26]

2.1.1 Additive manufacturing

Considering the high oxidability of Cu-Al alloy as well as the manufacturing trend of free-forming processes, additive manufacturing (AM) is an ideal candidate for manufacturing Cu-Al alloy with high quality. The first form of AM is creating a three-dimensional object layer by layer using computer-aided design (CAD), which was developed in 1980 by Hideo Kodama of Nagoya Municipal Industrial Research Institute [27]. AM actually is called by a joint name of rapid prototyping and rapid manufacturing but not a single technology concept. The innovation of these technologies was even recognized as the signal of the beginning of the third industrial evolution.

The advantage of RP contained time and cost reduction, human interaction, and consequently the product development cycle, also the possibility to create any shape

which is difficult for the manual fabricating [28]. Moreover, compared with the conventional manufacturing processes, AM is capable to fabricate components with more complicated geometries and competitive properties [29]. Thus, the application of this advanced technology is utilized in a wide range of area and the growth rate (around 24.1% in 2010) of AM applied in industry increased significantly [30].

The AM process can be divided into three part according to the type of raw material, including liquid based such as melting and polymerization, solid based like laminated object manufacturing (LOM) and powder based such as melting and binding. The liquid- and powder-based processes seem more promising than solid-based processes of which LOM is the predominant one nowadays. In 2004, electron beam melting(EBM), Prometal, laminated engineered net shaping (LENS), and Polyjet were not existent [31]. These technologies were first created to produce models, but they have expanded since then. A survey made by Wohlers presents 24 manufacturers participated and so did 65 services of more than 5000 users and costumers [32].

In terms of the specific application area, additive manufacturing technologies are capable to produce material with lighter structure which to some extent can reduce the weight of material. In this respect, it has gained more and more attentions in the aerospace industry which has high mechanical quality and low weight requirements as the component in aerospace industry suffers from high buy-to-fly ratio. Additionally, the advantage that AM is feasible to reproducing difficult-to-find part is appealing for the designers in the automotive industry. For instance, fabricating the parts for classic car

with high quality and accuracy was realized in previous work [33]. Moreover, additive manufacturing also contributes to the medical and art fields. Specifically, up to date, AM is possible to make a precise model of bone and accurate transplant with complicated structure before a surgery. Architects can utilize additive manufacturing to create 3D models for civil project.

By contrast, there are still some technical challenges to be solved although AM is promising in a wide range of area. Previous work detected the strength of products made by additive manufacturing. For example, as the powder-raw material is hard to melt absolutely, hole or even the cavity exists in the as-fabricated part, which would result in the brittleness of material. Furthermore, because of the restriction of machine for AM, it is not capable for every kind of common material especially metal. Even for the available materials, the standard such as parameters for various process in modern industry should also be accomplished. Additionally, for a lot of AM processes, machining processes are necessary for the as-fabricated components. Thus, the accuracy needs to be improved to reduce the cost of manufacturing.

To sum, AM technologies is already mature for fabricating nonmetal materials in a wide range of area such as ceramics and polymers, while there are a lot of research to be accomplished for metal material. In order to study the current status of metal AM, powder based and wire-feed additive manufacturing are reviewed in following sections.

2.1.1.1 Powder based AM

The powder-bed AM in modern industry mainly contains selective laser sintering (SLS), direct laser metal sintering (DLMS), electron beam melting (EBM), laser engineered net shaping (LENS) et al. and these technologies is capable to produce various material such as gold, silver, copper, aluminum and their alloys [34]. In powder-based additive manufacturing, a melt pool is created on the surface of substrate by the laser beam firstly and powder material is melted into. The subsequent deposition layers follow the scanning paths which is used to create the desired part geometry. Finally, machining process such as milling would proceed in order to eliminate the dimensional tolerance of sample [35]. The accuracy of fabrication can be controlled even reaching 30μm, as the powder is used as the raw material [36]. Comparatively, the distortion for powder AM is relatively low with the low linear deposit energy. However, the raw material for AM techniques are rigid and it is very difficult to customize the composition to satisfy the requirement of resulting components. Processes for fabricating metal powders are showed in Fig.2.2. Thus, the cost of commercially available metal powders is relatively high. The problems such as damage tolerance, surface roughness and inferior fatigue is still mentioned in previous work [37].

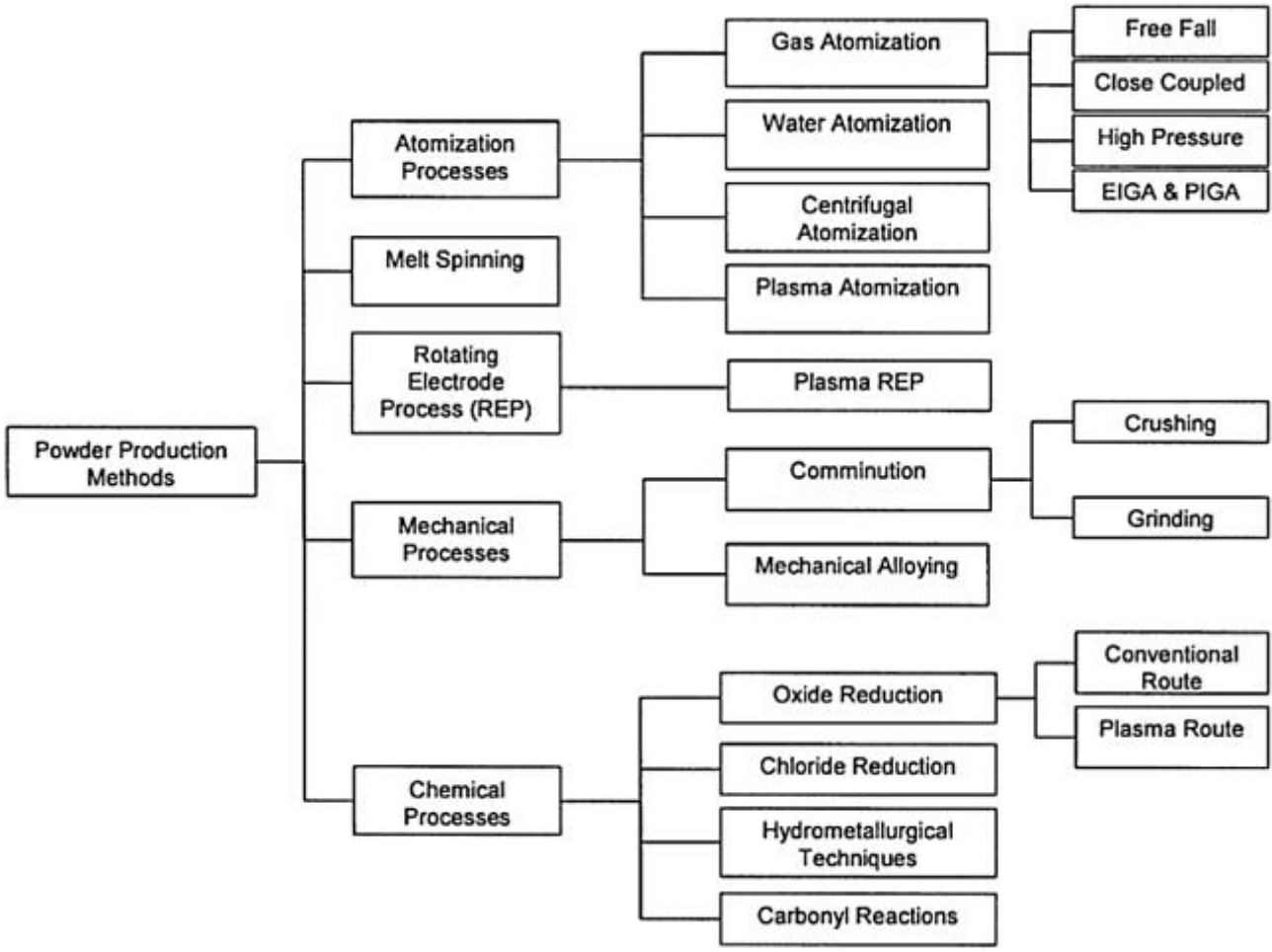

Figure 2. 2 Different processes for powder production [38]

Besides the problem of material, there are other limitations for powder-bed AM. For example, EMB takes place in a high vacuum chamber to avoid oxidation issues while the size of fabricating parts is limited. In the EBM processes, the contours of the target specimen are deposited which serve as the boundaries in order to separate with the surrounding metallic powder. Secondly, the middle part, normally showed as squares size, was fabricated along the contours. As mentioned, the whole process is worked under the vacuum chamber which is used to eliminate impurities and oxidation. Ultimately, the porosity lattice and scaffold helped to build up the bone structure. After the sample was cooled inside of the chamber, it must remove the remaining powder in a blast chamber via the powder recovery system [39].

In previous study, Heinl et al. reported that EBM possesses the capability to fabricate novel cellular Ti-6Al-4V structures especially in orthopedic applications according to the microcomputer tomography analysis [40]. The three-dimension structures Ti-6Al-4V with interconnected porosity is widely used for tissue ingrowth and vascularization. While it is modified with HCl and NaOH solutions, the implants presented apatite formation during bioactivity tests in simulated body fluid. EBM also is capable to fabricate Ti-24Nb-4Zr-8Sn porous components with 70% porosity, which was verified by Liu et al. in 2016 [41]. In contrast, besides the limitation of the vacuum size, it is understandable that the EBM process is hard to produce the full density material which is high demanded in modern industry. The existing porosity lattice would tremendously decrease the mechanical properties of component such as the hardness, tensile strength and ductility. The machines for EBM are just two type. One is Arcam® S12 and the other is Arcam® A2. And only titanium alloy and cobalt chromium are suitable for these machine [42].

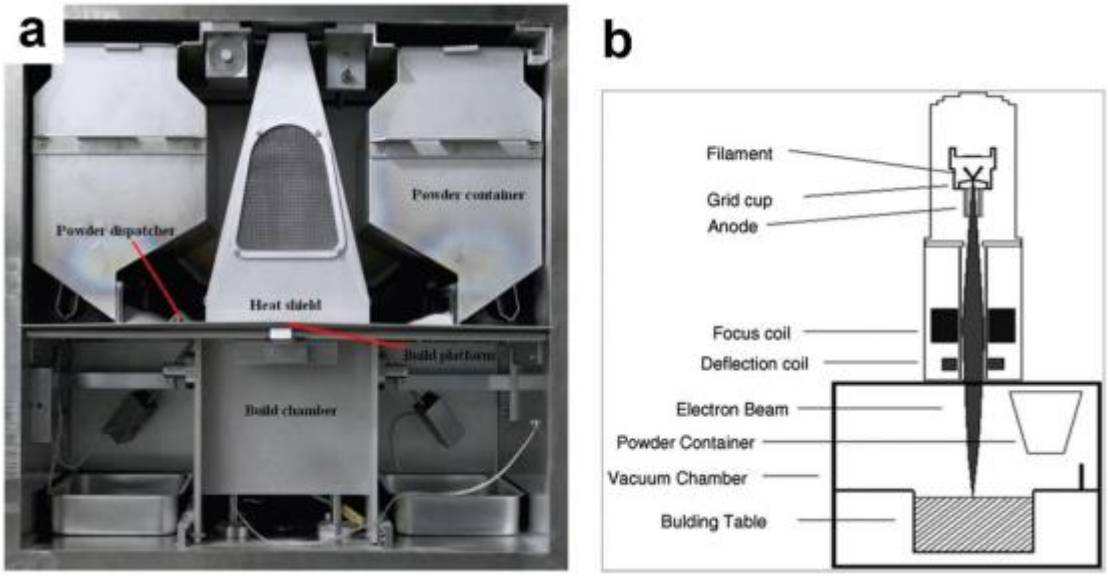

Figure 2. 3 (a) Fusion on an EBM machine; (b) Scheme of an additive machine [42]

2.1.1.2 Wire-arc additive manufacturing (WAAM)

Different with powder-based additive manufacturing, the filler material in wire-based AM is the typical welding wires. The wire-arc additive manufacturing was initially used to fabricate decorative items [43]. The hardware of WAAM contains the welding power source, torches and wire feeding systems. The motion can be controlled by either robotic systems or computer numerical controlled gantries [44].

This system had almost 90-year history and with the development of software such as robot control system it gains increasing research interest in the implementation of arc welding processes in large-scale manufacturing. The benefits of WAAM system contain the low cost, no need for vacuum chamber compared with electron beam method, large operating volume which is mainly depended by the envelope of robot, high deposition rate and less spatter. Besides that, wire-arc additive manufacturing also possesses the capability to fabricate large component with complex structure. Flanges and stiffened panel are usually produced by this promising technology.

Kazanas et.al reported the production of geometrical features using wire and arc additive manufacture with positional welding. The in-situ welding is widespread used for building features with limited accessibility without having to manipulate the part [45]. Besides the WAAM system the arc and gas metal arc welding (GMAW) and cold metal transfer (CMT) are also used in their work. They proved that the WAAM system

is capable to produce walls with various angles ranging from the vertical to horizontal positons, which means various shape can be fabricated. It is also possible to be used as hollow features when weight reduction is required in structures. In terms of the material, the feasibility of manufacturing iron and aluminum is certified. In this work, it is easy to find that WAAM is suitable to fabricate different shape and size products so as to satisfy the requirement of market. However, the basic properties of material were not presented. In this case, it is difficult to analyze the transform of crystal and even the density of product.

Ma et.al indicated fabricating the Ti-Al based alloy via the WAAM system. The gas tungsten arc welding process was utilized to deposit the intermetallic alloy in-situ from separate pure titanium and aluminum wire feed stocks [46].

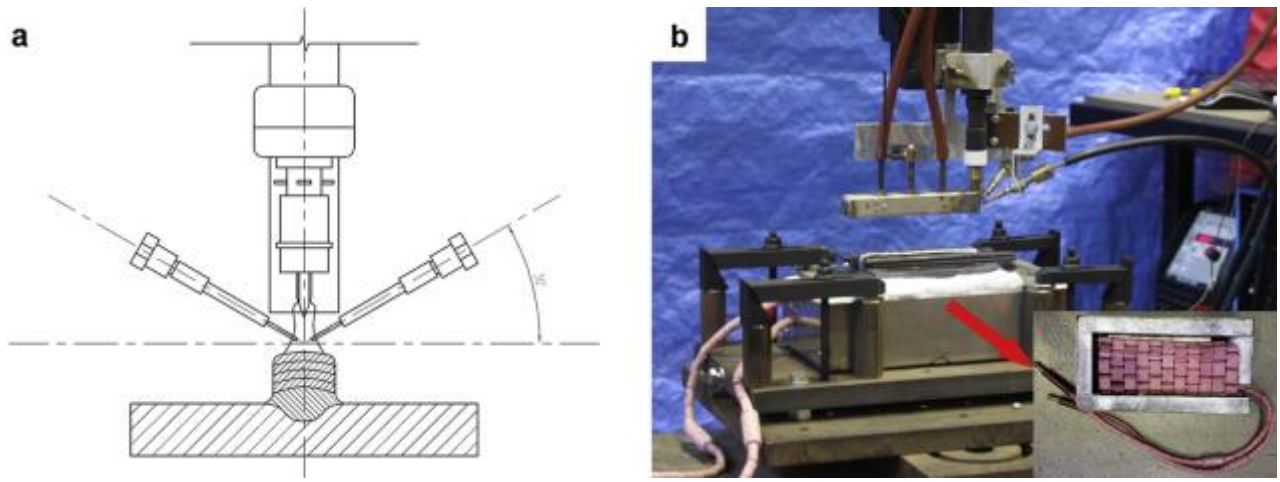

Figure 2. 4 Experimental equipment: (a) schematic drawing; (b) physical photo [16].

Fig. 2 showed the schematic drawing of the process, in which the the angle between two feeding nozzles is around 60° and in terms of the angle between the nozzles and basal

plate, it is 30°. As the two wire feeders was used in the system, the WAAM is capable to produce the intermetallic with various content of different element. Based on that, the application of WAAM is expanded. Furthermore, the characters of the as-fabricated alloy were detected.

According to grain shape and size, the material mainly presented as the columnar grains. The driving force of the columnar grain growth is generated by the temperature gradient during each single deposition process. Therefore, the preferred grain growth direction of the columnar grains is perpendicular to the direction of solid-liquid interface, which is the buildup direction. And as the buildup process continues, the melted metal in the subsequent deposition layers would continue to nucleate on the previous columnar grains and contribute to the grain growth. Besides that, the top region has a maximum hardness value and grain size is smaller than the middle and base part. It can be explained as that during the build-up process, the previous part was re-melted every time a new layer was deposited. For each time, the grain would follow the direction of heat driving force to grow again. The grain size would become larger. By contrast, at the top part, with fast solidification, the crystal in top part would not grow again. Thus, the grain size in the top part would become smaller. However, the inhomogeneous was also detected in these sample whereas the homogenization was not applied in the process.

However, WAAM system has a few challenges as the welding wire is chosen as the filler material. For example, the problems such as residual stress and distortion because

of the excessive heat input, relatively poor part accuracy caused by the “stair stepping” effect and poor surface finish of produced parts were studied in recent research [12]. Initially, the parameters of the fabricating process such as welding current, layer thickness, wire diameter, wire feeding speed and welding speed should be controlled carefully in order to achieve expectant geometrical shape and surface finish, especially for the large component with complex structure. Additionally, the deformations caused by residual stresses would lead to loss in tolerances and premature failure for large scale component in WAAM system. While fabricating large scale component, both process parameters, as mentioned before, and process planning significantly impacted on the thermal history of the part. Thus, part quality and part accuracy, such as surface finish and geometrical accuracy, should be carefully considered and designed.

2.2 Controlling of WAAM system

Generally, in order to check the feasibility of fabricating Cu-Al alloy via wire-arc additive manufacturing, the character of welding copper alloy should be studied initially. A successful welding process mainly depended on the microstructure of the welding material such as free of defects, having acceptable levels of residual stresses and distortion, the amount of spatter and the composition of target component [47]. However, the quality testing of these factor seems to be hardly measured. In this respect, the following controlling of the whole possess can be considered and studied such as cooling rate of molten pool, the amount and the concentration of heat input, the substrate material and the filler material so as to enhance the quality of welding process. As the characteristics of WAAM system is layer by layer, the heat transferred from the

torch to the welding pool and the thermal cycling on each deposition layer [48] have tremendous influence on both composition and mechanical properties of the products. Thus, the discussion of choosing power source for wire-arc additive manufacturing is important. In previous study, the power source for WAAM system mainly divided into gas tungsten arc welding (GTAW), gas metal arc welding (GMAW) and plasma arc welding (PAW) [49]. In order to comprehensively compare these heat source, GTAW and GMAW would be discussed respectively.

2.2.1 Gas metal arc welding (GMAW)

GMAW applies the consumable wire as the electrode forming an electric arc with the workpiece metal. The angle between torch arc and the substrate normally is 90°. GMAW is also known as the metal inert gas (MIG) welding process. In order to fabricate Cu-9at. %Al alloy, the GMAW with two wires also called tandem GMAW are reviewed in current research and the Fig. 2.5 exhibits the schematic tandem GMAW system.

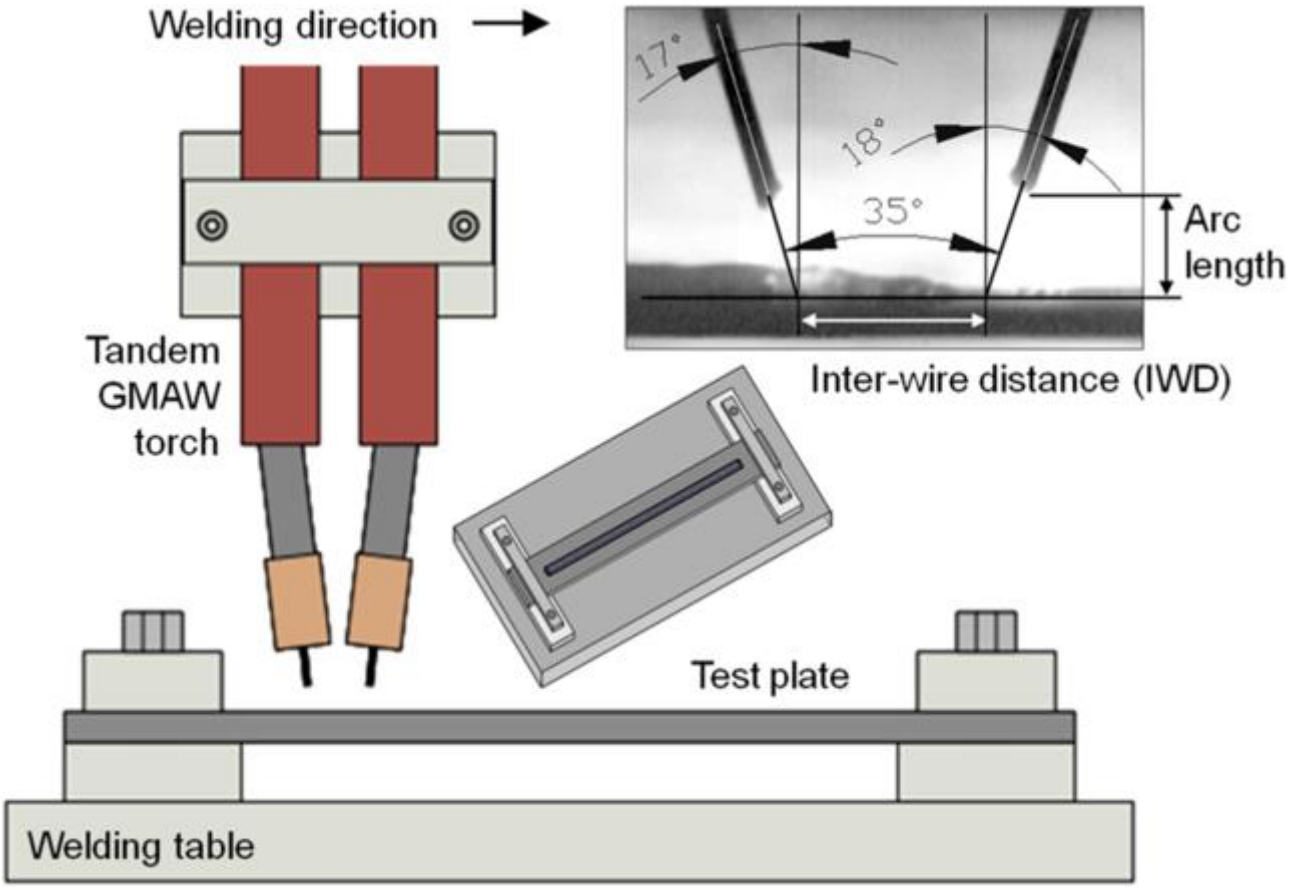

Figure 2. 5 Schematic experimental rig used for evaluating the Tandem Pulsed GMAW arcs [50]

In 1988, the tandem GMAW system was innovated to increase the welding penetration of the conventional GMAW. As shown in Fig. 2.5, the two wire electrodes are following the welding direction while the first one is served as the lead to open the welding pool and control the deposition rate and penetration. The following one mainly controlled the welding bead appearance. The two wires are individual controlling by two independent power source, although they are contributed to the same welding puddle. Furthermore, the lead and trail arcs may possess different operating modes according to the requirement of fabrication. Pulsed mode in T-GMAW is a good case in point. Because of the

development of the software for welding controlling such as the digital welding power sources, the T-GMAW with pulsed mode gains more interests in recent years. It has the capability to replace the submerged arc welding process (SAW) in shipbuilding industry. Fig. 2.6 showed the current of two arc which was controlled by the waveform and the whole welding process is relatively stable with less spatter even at the high travel speeds.

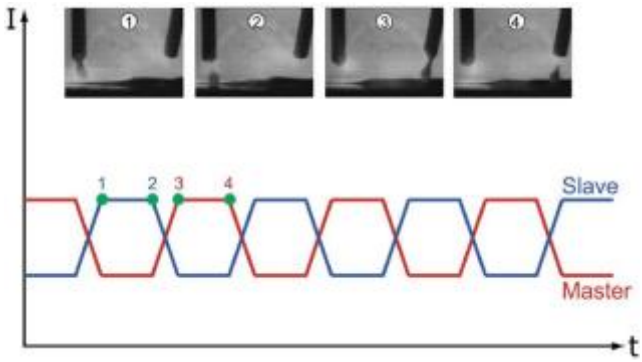

Figure 2. 6 Synchronous droplet removal in Pulse Tandem GMAW [51]

Nadzam in 2003 showed the advantages of T-GMAW including increasing the variety of products, less distortion, lower spatter and higher deposition rate, especially compared with traditional MIG welding process with single wire [52]. Besides that, T-GMAW system also was compared with SAW to fabricate S355 steel in 2008 and it also showed the similar benefits [53]. As one type of new welding process, the existing application of T-GMAW is for shipbuilding industry. Although this technology is already available for commercial application, researchers mainly tried to solve the stability problem of the welding pool. Especially for the material with high thermal conductivity such as copper, pulsed mode was used to avoid over heat input problem. In this respect, the whole system showed better performance and the problem of overlap of

peak pulses current between two arcs can be eliminated [54]. Furthermore, increasing welding speed of T-GMAW can also be achieved via synchronizing the two-wire pulse mode, while the weld deposition and penetration presents similar degree compared with GMAW without adversely effecting welding quality or heat input [53].

To sum, the tandem GMAW mainly possesses the advantage of high travel speeds, less distortion, high deposition rate and high quality weld deposits. However, the high spatter rate compared with GTAW system is one of the problem to solve. Especially for Cu-Al welding, the composition of aluminum is 9 at.% which required slow feeding speed for aluminum wire. In this respective, the spatter phenomenon during the welding process may lead to the inaccuracy of chemical composition. Additionally, the uniform of bead geometry is another problem. At the beginning and the end part of deposition wall, due to the inherent characteristics of GMAW system, the part accuracy and surface finish is hard to be achieved [55]. Thus, in this thesis, the power source of WAAM system choose gas tungsten arc welding (GTAW).

2.2.2 Gas tungsten arc welding (GTAW)

GTAW utilizes a non-consumable tungsten electrode serving as the welding torch and it is also well known as tungsten inert gas (TIG) welding process. The inert shielding gas such as argon or helium protects the electrodes, arc and welding area from oxidation or nitridation and filler metals are normally used.

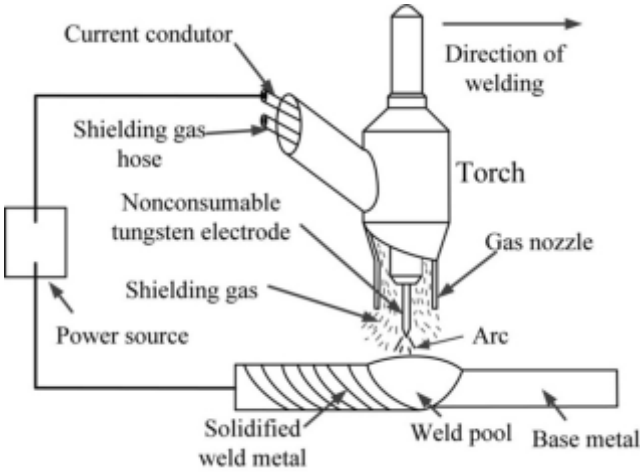

Figure 2. 7 Schematic diagram of GTAW system [56]

GTAW is widely used for welding stainless steel and non-ferrous metal such as copper alloy with thin sections. It mainly presents higher quality welds and no arc-welding fume compared with other welding processes such as shielded metal arc welding (SAW) and gas metal arc welding (GMAW) [57]. However, the conventional GTAW system is comparatively difficult to master for operator and the welding speed is relatively slower than other welding techniques [58]. While the GTAW is employed in AM processes, in order to improve the properties of material, a series of controlling methods have been developed.

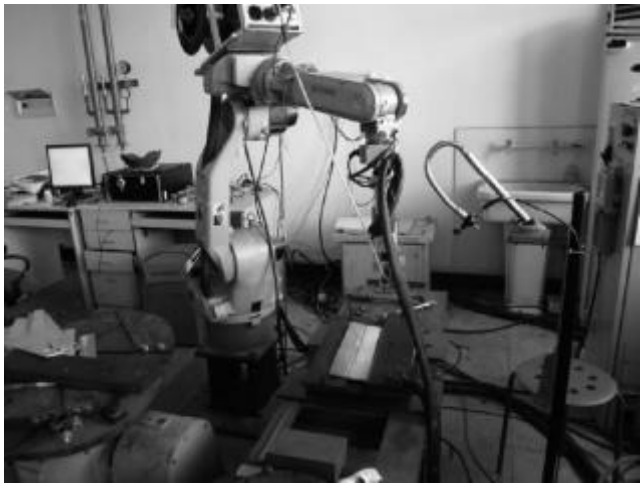

Figure 2. 8 The system diagram of GTAW displayed in robot [59]

In order to increase the application of the GTAW, air-cooled and water-cooled torches were innovated for welding under high current atmosphere. For the air-cooled torch, the current of welding usually attain at 200A while the counterpart can reach 600A in water-cooled system. At the same time, gas lenses and other accessories were created to protect the weld area from atmosphere contamination [60]. However, the overheated electrode and temperature transferring from the tungsten to welding target still existed. To address these problems, the negative polarity electrode was used while it was not suitable for non-ferrous materials such as aluminum alloy, which to some extent restricted the application of GTAW. Thus, the torch with alternating current mode was employed to stabilize the arc and fabricate Al alloy with high quality.

In 2004, Wang et al. fabricated three-dimensional cylindrical 4043 Al-alloy with 120 layers via GTAW in robotic system [61]. The build-up hollow cylindrical part showed good surface quality and excellent mechanical properties (the hardness of sample is around 50Hv). In terms of the microstructure of sample, it presented similar phenomenon with Ti-6Al-4V [16], which showed fine dendrite structure at the top layer

and coarse columnar grain in the middle and bottom part. In addition, the process parameters including arc voltage (arc length), welding current, welding speed and wire-feeding rate tremendously influence the geometry, microstructures, roughness and hardness of the build-up wall. In order to acquire appropriate parameters for GTAW system, in 2011, Bonaccorso et al. investigated the controller system for shaped metal deposition process [62]. Fig. 2.9 demonstrates a six-axis industrial welding robot with TIG welding power source. In particular, the welding process is mainly based on the NI Labview real time target architecture equipped with a pyrometer and a thermal camera. These cameras were mainly used for analysing temperature distribution and heating and cooling rate during the whole welding process. Additionally, welding camera, IR sensors and a microphone were also installed in the monitoring system. Based on the improvement of both software and hardware for controlling parameters, the stability of deposition process was relatively increased and became automatic. However, the microstructure and the mechanical properties were not involved in this research. The lack of additional shielding device may result in serious oxidization especially for aluminium which has high oxidability. Thus, investigating the influence of each controlling parameters on both microstructure and moulding is necessary.

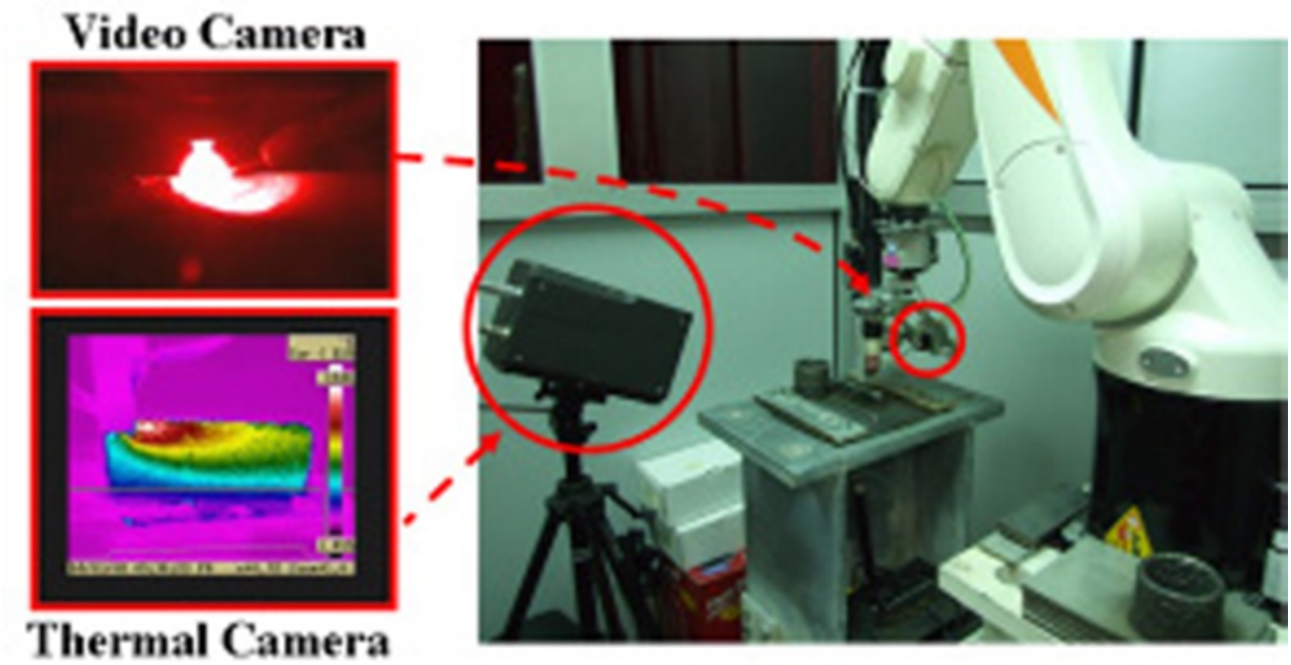

Figure 2. 9 The industrial robot with TIG welding equipped with sensors and camera [62]

2.2.2.1 Discussion of welding parameters

Besides arc voltage (arc length), welding current, welding speed and wire-feeding rate, the welding parameters also refer to shielding gas flow rate, preheating temperature and interpass temperature. In general, welding parameters mainly influence the dimensions such as penetration and width of the component and the mechanical properties and microstructure of sample. On the other hand, it also ensures the feasibility of fabricating multi-pass specimens especially net structure.

The selection of arc current depends on the thickness of substrate, material and the type of joint, as it directly influences the heat input and the penetration with the effect being proportional [63]. For material with high thermal conductivity, opening molten pool needs high heat input because of the diffusion of the heat during the beginning of

deposition. However, while an excess of heat is input to the deposition process, the height of wall would decrease and width would increase. If the accumulation of heat is too high, the collapse even happens on the top layers. According to the equation of resistance heat:

$$Q_R = I^2Rt$$

Q_R represents the resistance heat; *I* represents welding; *R* represents the equivalent resistance of welding arc and t represents the specific welding time on the deposition position. At the top layers, the heat input should be controlled to avoid collapse. According the heat input equation:

$$Q = \frac{I \times V \times \eta}{S}$$

Q is heat input; *I* is the welding current; *V* is welding voltage; η is efficiency of the welding process; *S* is the traveling speed. Normally, the efficiency of welding process (η) in direct current GTAW system is around 78% to 85% while it is relative lower in alternating current (68% to 85%).

Complementary with current, the welding heat input also influences the heat input according to the equation. In GTAW system, the welding current remains relatively constant and the voltage is responsive to the electrode-to-work distance. The increase of voltage mainly results in larger width and the decreasing of welding penetration. Additionally, long arc length is contributed to the melting of feeding wire and it is understandable that the operator can observe the molten pool more clearly. Short arc length usually cause short circuit because the feeding wire contact with the electrode and the contamination of the tungsten electrode. However, when the arc length is too long, the problem of porosity and inadequate shielding gas protection would generate

during deposition process. Thus, appropriate length of arc is almost equal to the diameter of electrode [64].

As in GTAW, current is constant so the appropriate voltage is depended on the current. The relationship is shown in formula below [65].

$$U = 10 + 0.04I$$

U is voltage; I is constant current. Under high current condition (over 600A), the safety welding voltage remains at 34V.

The traveling speed of WAAM should ensure that the arc can provide appropriate quantity of heat for the welding process in unit time. The welding material and welding directions are the main factors which influence the choice of welding speed. In GTAW, welding speed affects the width of molten pool and the depth of penetration. For materials with high thermal conductivity like copper alloys or non-flat work pieces, fast welding speed is selected to avoid large distortion and flowing of liquid metal [66]. In terms of cracking and oxidation susceptible materials, the welding speed is adversely slower as the cooling rate would increase with traveling speed. In addition, the excessive travel speed induces inadequate gas protection and incomplete melting of filler materials. Furthermore, traveling speed also have significant effect on the microstructure and mechanical properties of material. In 2014, Subravel et al. used GTAW to fabricate AZ31B magnesium alloy and various traveling speed were compared [67]. The joint fabricated at 135 mm/min expressed superior hardness and tensile properties compared with other specimens. The grain size in the fusion zone was refined under this condition. It can be explained as that the heat input level is found to

be optimum.

The flowing rate of shielding gas is an important factor for the morphology of GTAW bead. The choice of flowing rate is lied on the tungsten electrode diameter, while the diameter is depended on the welding current. With the increasing of current, the protection gas flowing rate should be improved in order to provide large scope of protection. Low flowing rate result in bad rigidity shielding gas, low wind resistance for out chamber welding and narrow protection area. By contrast, if the flowing rate is too high, the protection gas would be turbulence and the air may be involved into welding process hence the welding porosity, oxidation and nitridation is induced during the deposition process [68]. For the high thermal conductivity material, trailing shielding gas is recommended to ensure the welding bead is entirely under protection after solidification. Moreover, while argon is chosen as the protection gas, the relationship between flowing rate and welding speed should be considered. High traveling speed causes the excursion of argon because of the air friction. Consequently, the flowing rate should be slightly increased to provide desired protection.

The controlling of interpass temperature mainly based on the type of material, the thickness of substrate and heat input. The purpose of that is to control the welding cooling rate which has significantly effect on width of heat affected zone (HAZ) and the grain size. If the interpass temperature is too high, the grain size in HAZ would become large and reasonable, the mechanical properties such as hardness and impact toughness decreases tremendously. Inversely, the controlling of preheating temperature is mainly deceasing the cooling rate to avoid the generation of crack in HAZ. The relationship between interpass temperature and preheating temperature is that the interpass

temperature is normally higher or equal to the preheating temperature to avoid large distortion and cracks [69].

2.2.2.2 Filler material control

Compared with conventional welding material such as iron, nickel and titanium, welding for copper and aluminum is a pretty skill required job because of the bad welding properties of both materials. The challenge of welding copper is listed below [70, 71].

Refractory: Copper is one kind of material with high thermal conductivity. Especially at the first deposition layers, the molten pool is less inclined to be opened because of the conduction of heat. Thus, welding copper normally requires power source with high power, concentration of heat and preheating process.

- High mobility: Melting copper possesses high mobility, hence the work piece should be flat. Under the welding substrate, additional base plate is required to ensure the flat work piece.

- Ductile: Since the thermally expandable properties of copper, the shrinkage which to some extent decreases the effective width of component will be detected at the bottom of buildup wall. Furthermore, this kind of transformation is hardly inevitable if the method of compulsively preventing transformation is adopted, the dilution zone is more inclined to induce crack. Consequently, the tolerance of width should be considered while process design.

- Oxidability: Pure copper may react with outside atmosphere inducing Cu_2O or CuO which exist in grain boundary and eutectic is generated. It results in the decrease of mechanical properties like hardness and strength and corrosion resistance of welding wall.

- Generating crack: During the welding process, the expanding of copper induces tremendous stress in deposition region and the oxide exists in grain boundary. The wall is easy to generate crack. Additionally, the impurity element such as plumbum, bismuth, sulfur which would lead to crack should be avoid.

- Porosity: Argon should be selected as the shielding gas for copper alloy to avoid porosity. The solubility of hydrogen in liquid copper is relatively higher than that in solid copper. Thus, after cooling, the porosity is produced in the buildup wall, which induces bad mechanical properties and density.

In terms of aluminium, it possesses similar properties with copper, thermally expandable and high thermal conductivity [72]. Therefore, there are also some special requirements for aluminium welding. Initially, non-metallic Teflon liner should be used for wire feeding system in order to reduce the friction between wire and the liner. The driving roll for feeding aluminum wire should be U-groove instead of V-groove as U-groove driving roll can decrease the deformation and zigzagging during feeding process. Guiding device is necessary to be set as the entrance and exit of the liner to avoid the possible scratches on soft aluminum wire [73]. Besides the dedicated equipment, the oxidation of aluminum should be avoided. The melting point of Al_2O_3 is

relatively high and stable. Thus, it is hard to be eliminated in machining process. The existing of Al_2O_3 impeded combination of substrate metal and filler metal, which results in the impurity, defect and porosity. Normally, for aluminum welding, alternating current is utilized to avoid oxidation and trailing shielding device can be equipped along the torch at the same time. Relative oxidation principles of aluminum and copper are shown in below equations.

Copper: $2Cu + O_2 = 2CuO$

Aluminium: $4Al + 3O_2 = 2Al_2O_3$

Additionally, although controlling parameters of welding process can reduce the oxidation to some extent, extra grinding process is still required between each layer o ensure the deposition stability in the next pass.

2.3 Copper and Copper rich alloy properties

Pure copper is defined as containing minimum 99.3% copper content metal. As it is one kind of malleable and ductile material with excellent electrical and thermal conductivity, copper is widely utilized as building material, conductor of heat and electricity and marine hardware. The basic physical properties of pure copper are presented in Table 1.

Table 1 Physical properties of pure copper [74]

	Melting point (°C)	**Density (g cm^{-3})**	**Thermal conductivity (W m-K^{-1})**	**Elastic modulus (GPa)**
Pure copper	1083	8.95	391	117

There is no doubt that electrical conductivity is one of the most important property for the application of copper. It is mainly influenced by the thermal vibration and crystal defects which are caused by the additional atoms, dislocations and grain boundaries. With the increasing of these factors, the resistivity of copper would experience a decreasing and the electrical conductivity would be declined. On the other hand, the thermal conductivity of copper is also relatively higher, compared with other metals. In order to investigate the factors, the equation related to the ratio of electrical conductivity (k_{th}) is shown below.

$$k_{th} = \lambda LT$$

λ represents the Wiedemann-Franz law [75]; L represents Lorentz number and T represents the absolute temperature. According to the equation, the electrical conductivity is mainly affected by the temperature while it is less sensitive for the grain size.

By contrast, the use of unalloyed copper is mainly limited by the intrinsic low strength, low hardness and weak corrosion resistance. In the galvanic series, the corrosion resistance of copper is relatively lower than noble metals such as graphite, titanium, silver, passive stainless steels, and certain nickel alloys while above that of active nickel, stainless steels, tin, lead, cast irons, carbon steels, aluminum, zinc and magnesium systems. The galvanic series represents relative activities in seawater [76]. The mechanical properties are mainly depended on the crystal structure and copper has a face-centered cubic (FCC) structure which is shown in Fig.2.10. Although FCC structure materials usually possess high ductility and toughness, the strength and hardness is relatively lower without work-hardening process. To increase the mechanical properties of pure copper, various processes are used in previous studying, for example, cold working, solid solution hardening, precipitation hardening, dispersion strengthening, etc. while these approaches can significantly increase the strength, they will also lead to a pronounced reduction in conductivity. The challenge is to design a material with ideal combination of strength and conductivity.

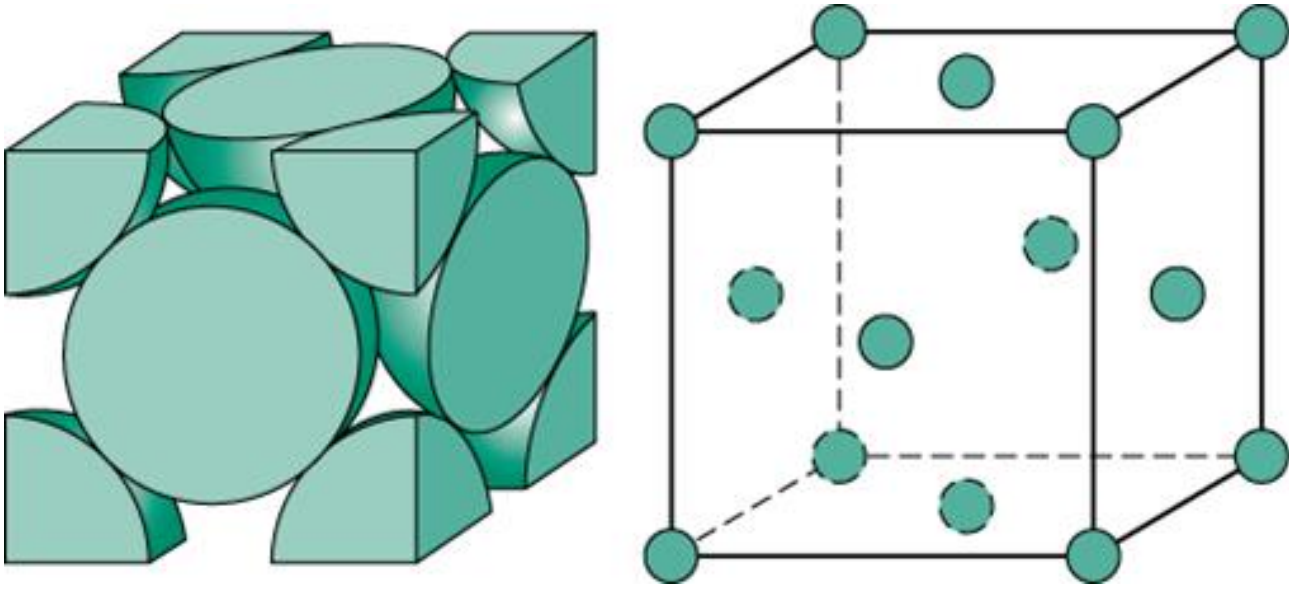

Figure 2. 10 Copper FCC structure

Cold working is an effective way to increase the mechanical properties (hardness and strength) of pure copper through decreasing the grain size while it slightly influences on the thermal and electrical conductivity [77]. By contrast, this machining process may also lead to soft structure while the temperature is around 200°C since copper can recrystallize at the low temperature [78]. In this respect, through controlling parameters of further machining process, ultrahigh-strength copper with comparable conductivity at the same time can be induced, which was also proved in previous work. For instance, nanoscale twin crystal can be generated by cold working in FCC structural copper [79] and the grain size would decrease tremendously. According to Hall-Petch relationship, both hardness and tensile strength of copper can be improved although the ductility would decrease slightly. While the grain size have slight effect on conductivity which is mention before, the excellent mechanical properties can broaden the application of copper in industry.

Alloying is another feasible method to improve the mechanical strength significantly. Compared with cold working, alloying possesses the advantage that it can raise the softening temperatures, while the electrical and thermal conductivity is relatively lower because of the effect of additional elements. The function of alloying is altering the structure of copper, which can induce three type of alloying strengthening including solid solution hardening, precipitation hardening and dispersion strengthening. In present work, solid solution hardening is selected as the method to enhance the properties of copper.

2.3.1 Copper and aluminum binary system

So as to improve the mechanical properties of copper, solid solution strengthening is a effective methods. Thus, aluminum is one of the ideal candidate. Copper-aluminum alloys are mainly used for oil and gas pipelines, heat exchangers, propellers, valves, gate valves and laminated plates for small boats' steel hulls [1]. While the content of aluminum is lower than 16.8 at.%, it has excellent resistance to corrosion for the marine industry. Besides that, the prominent characters, such as low cost, high deposition rate, excellent adhesion and good resistance to oxidation, also make Cu-Al alloys gains more attention in previous research.

The aluminum serving as the solution-solid elements is mainly to decrease the stacking fault energy. Based on that, the twin crystal is more likely to be produced and according to the Hall-Petch relationship, while the grain size is decreased, the hardness and

strength would experience a significant increase. In order to generate the ultrafine-grained, various severe plastic deformation techniques have been widely developed to produce the ultrafine-grained or even the nanostructured materials that can be used in a wide range of structural applications.

X.H. An et al detected the microstructure and shear fracture of Cu-16 at.%Al which was induced by the equal channel angular pressing (ECAP) [80]. The grain refinement processes during ECAP generally originate from the accumulation, interaction tangling and spatial rearrangement of dislocations in the metals with medium or high stacking fault energy(SFE), and the subdivision of original coarse grains is operated by twin fragmentation in the materials with low SFE. In terms of the purpose of their research, it mainly focuses on revealing the main factors leading to the shear fracture, the microstructure evolution of Cu-Al alloy. Furthermore, it also documented the property of materials and external deformation factors in grain refinement. As a result of the low SFE of Cu-Al material, the plastic deformation and the accommodation of the shear strain would transform from the dislocation slip and stacking faults to the micro shear bands on the original grain of Cu-Al alloy. To sum, the cold working process would result in the improving of hardness and twin would be generated. However, there are some gap in this work. For example, the commercial Cu-16at.%Al rod was used to the ECAP, but technology of manufacturing the raw material was not presented. To some extent, both mechanical properties and microstructure are determined by the process of fabrication. Without the introduction of process, it is hard to show the transformation after ECAP. Thus, in order to document the benefits of ECAP, the comparison between raw material and pressed material should exhibit.

In order to investigate the influence of aluminum content on mechanical properties, Tao et.al introduced deformation twins into the matrix of pure Cu with medium stacking fault energy(SFE) of 78 mJ/m^2 and copper alloying with 5 at.%, 10at.% and 15at.%Al respectively[3]. With the increasing of aluminum content, the SFE of Cu-Al solid solution experienced a dramatically drop from 78 mJ/m^2 and to5 mJ/m^2. The lower SFE means that the original material has higher possibility to transform to defect structures after the plastic deformation. In this work, split Hopkinson pressure bar(SHPB) with the strain rate of 10^3/sec was utilized to deformation diminutive twins. In terms of the hardness testing, it showed an improving trend with the increasing of Al content, while the hardness of Cu-15 at.% Al which is around 2300 MPa is almost twofold for the hardness of pure copper. It is also interesting to note that for Cu-10 at.% Al and Cu-15 at.% Al, the hardness just increases by 200 MPa. Based on that, the increasing micro-hardness is attributed to the solid solution strengthening effect of Al, and due to the formation of deformation twins, while the deformation twins possess larger influence on micro-hardness [2].

In previous work, the properties of original Cu-Al alloy were also discussed. Fabricating homogeneous Cu-Al solid solution without other intermetallic such as Al_2Cu and Cu_9Al_4 is important during the manufacturing process. Duina et.al reported the phase and microstructure evolution of the Cu-13 wt.% Al mixture during treatment in a high-energy planetary ball mill with a particular focus on the early stages of mechanical alloying. If insufficient energy is supported during the producing process, Al_2Cu and Cu_9Al_4 would be produced in Cu-Al alloy even when the content of Al is

lower than 2 at.% [9]. Also, it has been confirmed that during the powder milling procedure of Cu-Al alloy, θ-Al_2Cu and γ-Cu_9Al_4 phase would be firstly generated when Cu and 14 at.%Al are mixed; then with the proceeding of ball-milling or homogenization, the Al_2Cu phase and Cu_9Al_4 phase would transform into Cu-Al solid solution alloy [81]. In addition, the oxide such as CuO and Al_2O_3 are not detected in the XRD pattern. Without the protecting method during the process, the high energy of ball mill and the instinct property of Cu and Al, which has low resistance of oxidation, lead to the impurity. Thus, it showed that while producing the Cu-Al alloy, some protecting measure such as protecting gas or even vacuum environment is necessary. Besides that, the shortage of ball milling is that iron particles which comes from the milling machine would mix with the Cu-Al. It mainly results in the brittleness of alloy and inaccuracy of mechanical properties testing.

2.3.2 Heat treatment for Cu-Al

Homogenizing annealing is one type of heat treatment to homogenize the chemical composition and phase. The purpose of homogenization is that during annealing, the elements in the alloy are solid-state diffused and the segregation can be eliminated, especially for the producing process with high cooling rate such as welding. Generally, the temperature is slightly lower than the solidus temperature (150-300°C) and the time for heat treatment is decided by the type and size of component. After annealing, the specimen is cooled naturally with the furnace. However, the homogenization process is energy consumption and high cost. While homogenizing steel, as the time for annealing is long (10-15h), the grain size will increase and in order to refine the grain, the full annealing or normalizing process should be adopted. Additionally, grain boundary

migration also may happen during annealing process. Grain boundary migration refers to the movement of boundary separating two grains. The movements take place by the diffusion of single atoms from one grain across the boundary to the other grain. This motion results in the migration of the boundary in the opposite direction to the diffusion direction [82]. The speed of migration is depended on the temperature and the boundary curvature. With the increase of temperature and decreasing of boundary curvature, the speed of migration to the center of curvature would improve.

In previous study, Al_2Cu phase and Cu_9Al_4 phase has been observed in Cu-Al fabricating process. In 1993, Jiang et al. reported the interfacial reaction of copper rich Cu/Al multilayer films (10 at.% Al) which was investigated by differential scanning calorimetry (DSC) and transmission electron microscopy (TEM) [83]. Initially while the temperature is lower than 620K, the material showed thermal stability and the films did not grow. With the increasing of temperature, the sequence of reaction would happen.

$$Cu + Al \rightarrow CuAl_2$$

and then

$$Cu + CuAl_2 \rightarrow Cu_9Al_4$$

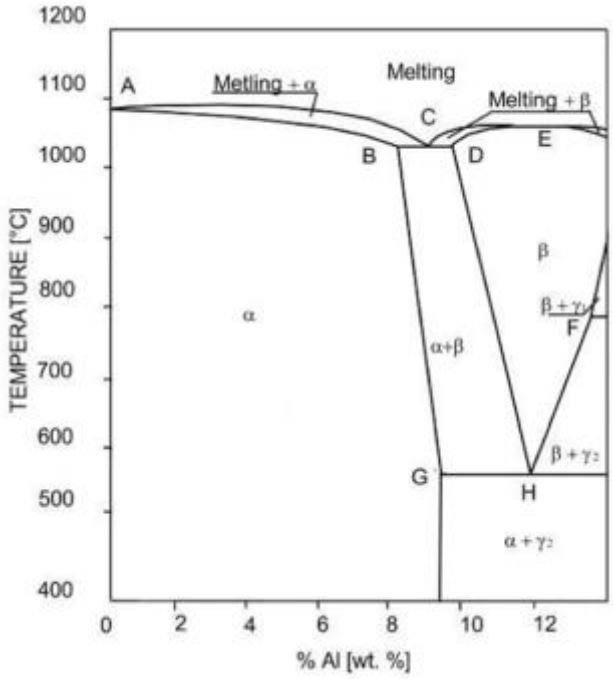

Figure 2. 11 Cu-rich Cu-Al system equilibrium phase diagram

The first process would be quickly finished because of the exhaustion of Al. However, according to the equilibrium phase diagram Fig.2.11, there should be only Cu-Al solid solution. The activation energies for the formation of each phase explained this phenomenon. For solid solution, the activation energy for interfacial diffusion of Al in Cu is 0.87 eV on the basis of the study by Shearer et al. [84], which is higher than the counterpart of formation Al_2Cu phase and Cu_9Al_4 phase, 0.78±0.11 and 0.83±0.02 respectively. The low value of activation energies for formation the Al_2Cu and Cu_9Al_4 is due to the fact that the interfacial reactions in Cu/Al multilayer film are chiefly controlled by the cooperation of interfacial diffusion and grain boundary diffusion.

In order to eliminate the impurity, high energy process was utilized. For example, Ying and Zhang in 2000 investigated fabricating Cu-14 at.% Al and Cu-35 at.% Al via ball milling process [81]. The characters of material which is milled at 1h, 2h, 4h and 8h was

studied. Additionally, the temperature for heat treatment ranged from room temperature to 650 °C and the heating rate was 20°C/min. For low Al composition alloy, with the increase of ball milling time and heat treatment, solid solution forms as a result of mechanical alloying. It showed that alloying between Cu and Al can be achieved either via ball milling or heat treating the milled powder. Furthermore, they also reported that the first phase generated by ball milling are Al_2Cu and Cu_9Al_4 because it is easier for θ-Al_2Cu and γ-Cu_9Al_4 to nucleate at the Cu/Al interfaces. In 2002, Dubourg et al. presents the mechanical characterisation of Al-Cu laser alloying and the effect of annealing process upon the microstructure and mechanical properties were investigated [85]. An annealing of 480°C for 24h was utilized in their research. The annealing made the eutectic coalescence with the primary grains and it decreased the micro-hardness of material while increased the elastic modulus. The result was mainly caused by the growth of grain. While the grain size increased, the hardness and strength would decrease and the elastic modulus would increase inversely.

2.3.3 Twin crystal in FCC structure materials

Crystal twinning occurs when two separate crystals share some of the same crystal lattice points in a symmetrical manner [86]. The result is an intergrowth of two separate crystals in a variety of specific configuration. A twin boundary or composition surface separates the two crystals. The theory of generating twins in FCC structural material is exhibited in Fig.2.12.

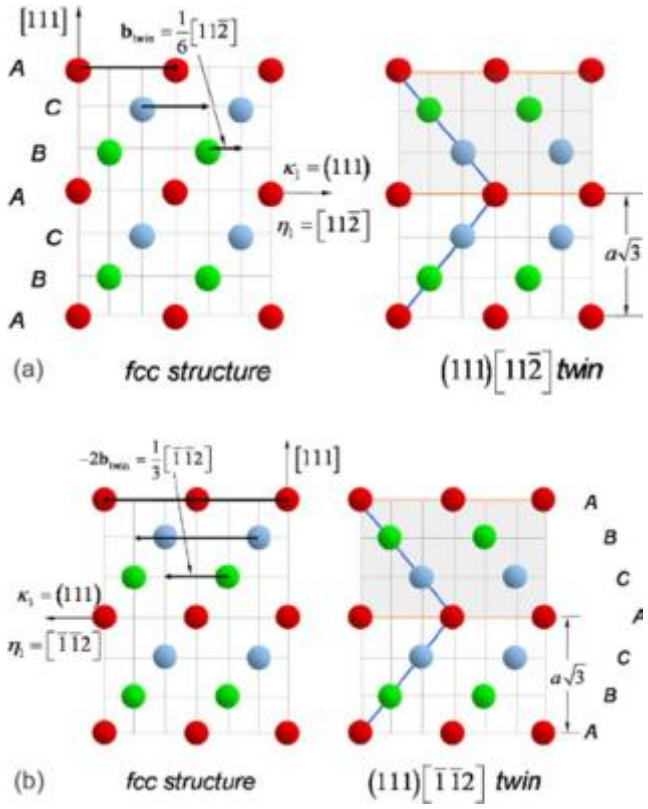

Figure 2. 12 Schematic of two opposite FCC twinning modes [86]

Nucleation of twins in FCC materials occurs due to passage of Shockley partial dislocations successively. Especially the (111) planes in FCC structure, it permits twinning shear in 7 direction except the opposite direction. The twin crystal is mainly divided into three types according to the mechanism of formation, growth twins, annealing twins and deformation twins respectively. For Cu-Al binary alloy, annealing twins and deformation twins gained more interests in previous study.

In terms of annealing twins, during the cooling process, crystal system becomes unstable and crystal structure must re-organize or transform to another more stable form. The evolution of crystal during the annealing process depends significantly on the characteristics of the metal such as the stored energy, the grain boundary structure and

the grain size [87]. The driving force for formation of twinning structure is the reduction in the Gibbs free energy in the system [88]. In 2009, Cahoon et al. reported adopting a quantitative approach to understand the parameters that influence the density of annealing twins [89]. The density of annealing twins referred to the number of twins per unit length p. The phenomenological equation is shown below.

$$p = C_3 \frac{\Delta G^0}{\gamma} \ln \frac{d}{d_0}$$

C_3 is a dimensionless constant; $\Delta G^0$is the difference in the Gibbs free energy between the growing and shrinking grain; γ is the stacking fault energy; d is the grain size and d_0 is a critical grain size below which twins will not form. According to the equation, the increasing of annealing twins is mainly depended on the decreasing of stacking fault energy (SFE) and grain size. Furthermore, the existence of high residual stresses in FCC metals during annealing contains a higher fraction of annealing twins [90].

For deformation twins, it is the result of stress on the crystal after the crystal has formed. In FCC structural material, SFE affects significantly the deformation mechanisms during high-strain deformation by cold rolling or severe plastic deformation. When the SFE is low, dislocation slip behaves in the planar form and dislocation recovery is inhibited [91]. Besides that, the deformation microstructures were also detected in tensile testing.

2.4 Summary and scope of the work

In this chapter, a comprehensive introduction of AM, power source for WAAM and researches on Cu-Al binary system are presented. Additionally, the homogenizing annealing process and formation of twin are reviewed to support the present subject.

In general, AM process is capable to produce a three-dimensional component in which successive layers of material are fabricated by controlling of computer. The advantage of the AM system is time and cost reduction, human interaction, and consequently the product development cycle, also the possibility to create any shape which is difficult for the manual fabrication. The AM processes are mainly divided into powder based and wire-feed process according to the type of filler materials. Compared with powder-bed AM process, wire-feed AM such as WAAM system is appealing for fabricating Cu-Al alloy since it has the capability of fabricating full density material with lower cost of filler material and equipment. However, the problem of WAAM system like residual stress and distortion in the substrate, lower manufacturing accuracy and the oxidation of active material should be solved by controlling the deposition parameters.

In terms of fabricating material, copper alloy mainly possesses high electrical and thermal conductivity and excellent ductility. While aluminum serves as the additional element, the corrosion resistance and wear resistance can be significantly improved and the stacking fault energy will be reduced. However, the low hardness and strength are the major disadvantages obstructing the application in modern industry. Up to date, the manufacturing process for copper-rich Cu-Al alloy contained powder metallurgy processes such as induction vacuum melting, furnace arc melting and ball milling. Since it has been stated from previous research that innovative processing and reduction of manufacturing cost is a main research focus of Cu-Al binary material, the WAAM

process is utilized to fabricate Cu-rich Cu-Al alloy. The feasibility, mechanical and material properties of deposition structures are investigated in the following chapter.

After the review of previous work, in Chapter 3 the setup for fabricating Cu-Al alloy, specific parameters and sample preparation are investigated. In order to detect the microstructure and mechanical properties, optical microscope (OM), X-ray diffraction (XRD), energy dispersive spectrometer (EDS) and scanning electron microscope (SEM) were used.

In Chapter 4, 5 and 6, the macro and micro structure of Cu-9 at.%Al including as-fabricated, annealed at 800°C and annealed at 900 °C samples are analysed. The phase characterization is investigated by XRD to exhibit the phase transformation after annealing process. Subsequently, the composition of Al is shown to verify the feasibility of fabricating Cu-Al alloy. Hardness and tensile testing are proceeded to show the mechanical properties of Cu-Al produced via WAAM system.

To sum, the aim of this research subject is to apply WAAM process to in-situ fabricate Cu-rich Cu-9 at.%Al and further develop the process. At the same time, the influence of annealing process for Cu-Al alloy fabricated by WAAM system is studied.

Chapter 3 Experimental setup

3.1 Hardware setup for Cu-Al alloy deposition

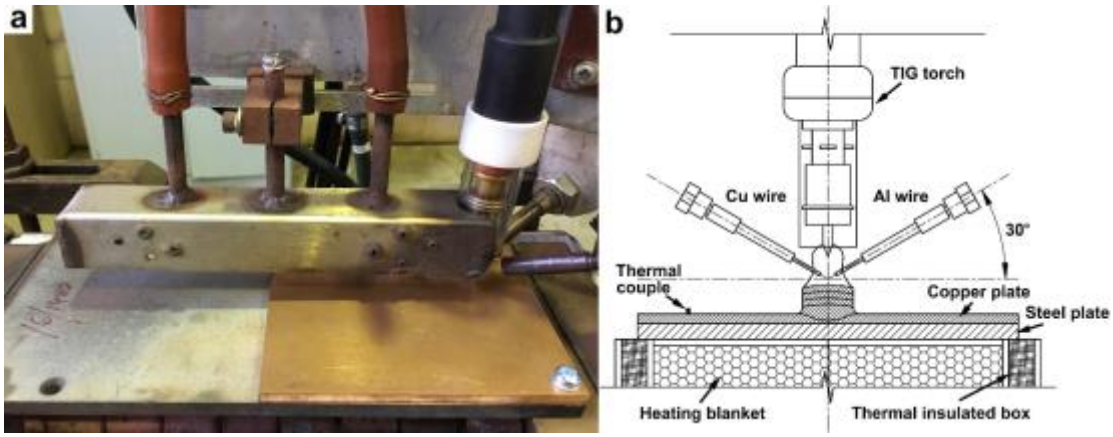

Figure 3. 1 WAAM process setup for Cu-Al alloy: (a) physical photo; (b) schematic drawing.

The setup of the WAAM process used for fabricating Cu-9 at. % Al is shown in Fig.3.1. The deposition power source was provided by a Kemppi Master TIG MLS 2000. The deposition current was 160A and the arc length was 3.5 mm, to ensure sufficient local heat input for opening the molten pool on the pure copper substrate. The two wire-feed nozzles, one for ø0.9 99.9%-purity copper wire and another for ø0.9 1080 grade aluminum wire, had independent wire-feed controls in order to adjust the chemical composition in the deposition process. The 3-dimension positions of the TIG torch, two wire-feed nozzles and the substrate are shown in the physical photo (Fig.3.1a). As shown in Fig. 1b, the angle between the wire-feed nozzles and substrate was 30°. The wire-feed speeds of Cu and Al wires were 1300 mm/min and 311 mm/min, respectively. And the

average deposition energy was controlled at 20.2 kJ/g in order to ensure the deposition stability. The travel speed was set at 95 mm/min, which is relatively slow to ensure sufficient deposition line energy and the continuity of the deposition beads. After each single deposition, grinding process was applied to clean the deposition surface for the subsequent layer.

In order to open the molten pool on the copper plate, the interpass temperature was set at 400°C. It was achieved using a heating blanket set in an asbestos thermal insulated box as shown in Fig.3.1b. The interpass temperature was accurately monitored and controlled using two K-type thermal couples, one was connected to the preheating machine itself, and the other was connected to the monitoring software in the computer using a signal converter. The detailed deposition parameters are listed systematically in Tab. 2.

Table 2 Deposition parameters of the WAAM process for 9 at. % Al Cu-Al.

Parameter	**Unit**	**Value**
Deposition current	A	160
Arc length	mm	3.5
Cu wire feed speed	mm/min	1300
Al wire feed speed	mm/min	311
Deposition energy	kJ/g	20.2
Travel speed	mm/min	95

Interpass temperature	°C	400

In addition, same as in the fabrications of Fe-Al and Ti-Al alloys [11, 46], pure argon was used as the inert shielding gas for the entire deposition process. And besides the gas shielding from the TIG torch, an additional trailing gas shielding box as indicated in Fig. 1a, was applied with a gas flow rate of 9 L/min to protect the as-fabricated deposit from oxidation during cooling.

The copper substrate was chosen as 3 mm in thickness and 100 mm in the other two dimensions. In order to prevent the copper substrate from being penetrated and deformed by the high-energy torch, the substrate was fixed on a 5 mm DH36 steel plate as shown in Fig. 1b. Considering the extremely high thermal conductivity of the copper, during the actual fabrication, the TIG torch would turn on and travel on the copper plate without filler wires for once to create a local high temperature and ensure the molten pool opening for the subsequent material depositions. In summary, the high deposition current and interpass temperature, thin thickness of copper substrate, low torch travel speed, and the one-time torch run before material deposition, are all designed to ensure the molten pool opening in the process. Finally, 15 layers were deposited in the buildup wall.

3.2 Sample preparation and test

Three cross section samples were extracted from middle part of the fabricated wall using wire electrical discharge machining (EDM) for further heat treatment and material

characterizations. The heat treatments were conducted using a KTL 1400 tube furnace which is shown in fig. 3.2. Two heat treatment conditions were applied to homogenize the as-fabricated material: one was annealed at 800 °C and the other was annealed at 900 °C, the annealing time for both methods are two hours. The furnace was first heated up to the required temperature before the sample was put in. And the samples were taken out from the furnace right after two hours and air cooled to ambient temperature. Pure argon gas was used during the annealing processes. For the convenience of future discussion, we name the as-fabricated sample as Sample 1, the sample heat treated at 800 °C as Sample 2, and the sample heat treated at 900 °C as Sample 3.

Figure 3. 2 KTL 1400 tube furnace

The sample for OM was initially cut via Struers® Accutom-50 cutting machine installed standard Struers® 50A13 aluminum oxide cutting wheel so as to cut the extra substrate of specimens to make it fit for the mounting process afterwards. Considering the hardness of pure copper, researchers set the rotation speed of the wheel at 5000rpm.

Additionally, the feeding force limit was set as “medium” with a feeding speed at 0.03mm/s in order to protect the cutting wheel.

Figure 3. 3 Struers® Accutom-50 cutting machine in present study

The specimens were hot mounted by Struers® CitoPress-20 hot mounting machine with Struers® PolyFast powder which is eligible for the following SEM examination.

Figure 3. 4 Struers® CitoPress-20 hot mounting machine in present study

The grinding and polishing of the sample were conducted on a Struers TegraPol-21 automatic polishing machine. Considering the low hardness and surface sensitivity of Cu-Al alloy, after being grinded to P1200 by silicon papers, the cross-section specimens

were polished using 6 μm Mol, 3 μm Mol, 1 μm Mol and finally the active oxide polishing suspensions (OP-S). Afterwards, the samples were etched using hydrochloric acid ferric chloride solution for two seconds to reveal the microstructures. The microstructures of the cross-section samples were acquired using a Leica MMRM research microscope. For general microstructures, the photos were taken under grayscale mode, while in order to reveal the twins more clearly in the top surface, the photos of the twins near the top surface were taken under color mode.

Figure 3. 5 Struers TegraPol-21 automatic polishing machine in present study

The hardness along the vertical centerline of three cross-section samples were measured at a load of 0.4 kg with 0.5 mm intervals and an indentation time of four seconds. Subsequently, the chemical composition along the same line of the three samples were characterized using a JEOL JSM-6490LA scanning electron microscopy (SEM)

equipped with an energy dispersive X-ray spectrometer (EDS) at 20 kV, the characterization points were set right aside the hardness testing points.

The consequences of homogenizing heat treatments were estimated according to the content of Cu-Al intermetallic phases such as $CuAl_2$ and Cu_9Al_4. The phase characterization was conducted using a GBC MMA X-ray diffractometer (XRD) with CuKα radiation (=1.5418 Å). Afterwards, tensile tests were performed to the as-fabricated material and the one was better homogenized by the heat treatment, in order to evaluate the mechanical property improvement after the heat treatment. For each case, four tensile specimens were extracted from the middle section of the buildup walls, in order to obtain effective results. The tests were conducted using a MTS 370 hydraulic load unit at a constant strain rate of 5×10^{-3} s^{-1} under room temperature. The gage volume of the tensile specimens is 10 mm × 2 mm × 1.5 mm. The fractured surfaces were investigated under SEM, and the microstructures near the fracture were observed by polishing and etching the fractured specimens.

Chapter 4 Microstructural evaluation and phase characterization

4.1 Microstructural evaluation

According to the feature of microstructure for buildup wall, the specimens can be divided into four sections: substrate, dilution zone, middle region and top region. In general, according to the previous study, the microstructure in the bottom dilution zone of sample fabricated via wire-arc additive manufacturing was relatively complex because of the diffusion of substrate material. It mainly presented slender dentrite perpendicularly to the substrate. With the increase of the deposition height, the buildup wall mainly normally exhibited large columnar grains in the vertical build up direction in the middle region. Moreover, due to the preheating effect of the former layers on the latter ones, the heat was accumulated gradually until a thermal balance was reached. As a result, the grains grew at almost the same speed along each direction, eventually forming the equiaxed crystal on the top region [92].

In order to detect the specific microstructure of Cu-Al samples, Leica® DMRM optical microscope was used in present research which is shown in Fig.4.1. By using grayscale mode, the precipitate and grain boundaries can be clearly observed. By contrast, colourful mode was utilized to observe the twinning structure morphology in the top region.

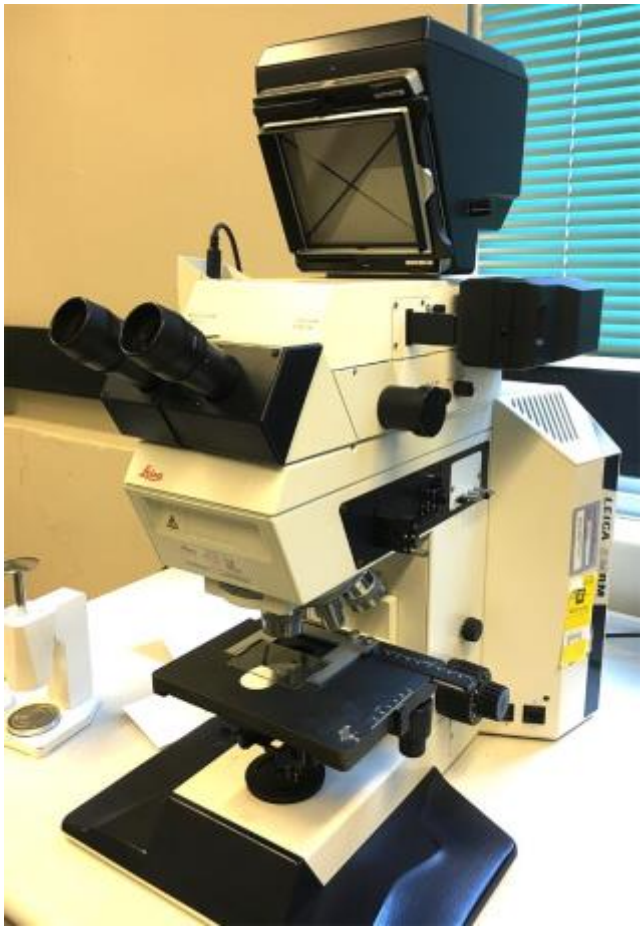

Figure 4. 1 Leica® DMRM optical microscope

4.1.1 Result and discussion

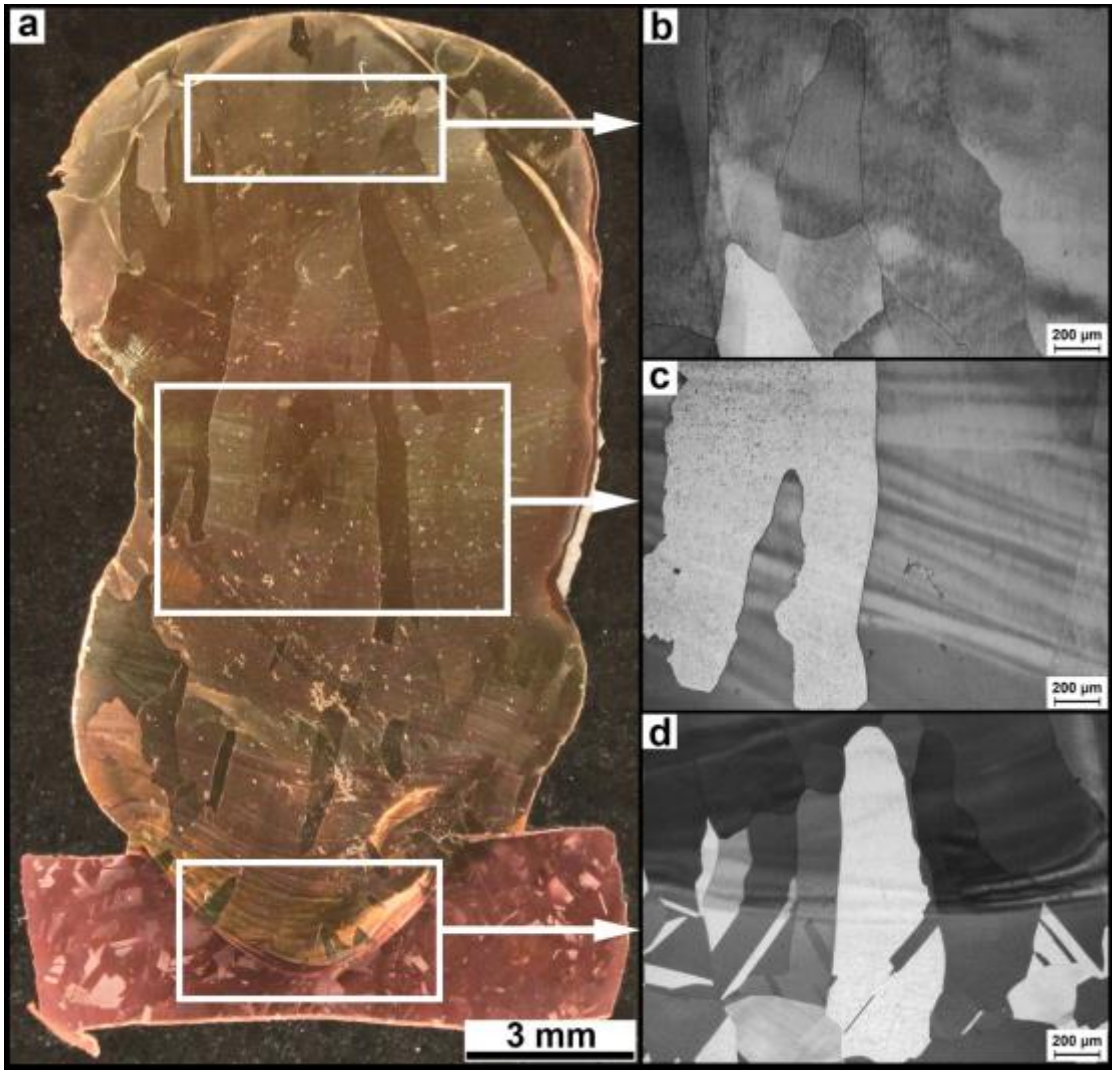

Figure 4. 2 Macro and micro structures of the as-fabricated cross-section sample (Sample 1): (a) the macrostructure; (b) microstructure in top section; (c) microstructure in middle section; (d) microstructure near the boundary line between dilution area and base mat

As shown in Fig.4.2a, the macrostructure of the Sample 1, there exhibits obvious shrinkage in the very bottom region, which decreases the effective width of the wall. This defect is caused by the difficulty to open the molten pool during the first few layers

of deposition due to the extremely high thermal conductivity of the copper substrate. The macrostructure of the as-fabricated buildup wall consists of large epitaxial columnar grains in the middle region (Fig.4.2c), and relatively equiaxed grains in the top region (Fig.4.2b). This is the typical grain structure generated by the WAAM process, which is basically a multi-pass arc welding process. The driving force for the columnar grain growth comes from the temperature gradient during each layer of deposition. Therefore, the preferred grain growth direction is along the buildup direction, which is perpendicular to the direction of solid-liquid interface. And as the buildup process continues, the melted metal in the subsequent deposition layers would continue to nucleate on the previous columnar grains and contribute to the grain growth [46].

Fig.4.2 d shows the microstructures near the boundary of substrate and buildup material. It clearly exhibits the crystal transformation from typical copper twinning in the substrate to remolten columnar grains in the dilution affected zone. The relatively small columnar grains above the boundary in Fig.4.2 d are the columnar prior grains function as the nucleuses of the following grain growth [93]. Although the buildup Cu-Al alloy has low stacking fault energy and the high tendency to have twinning, no such structure is found in the buildup material under as-fabricated condition. This is because neither plastic deformation nor annealing with enough time duration was applied to Sample 1, although the multi-depositions of WAAM process can be considered as short-time annealing processes to the previous buildup material.

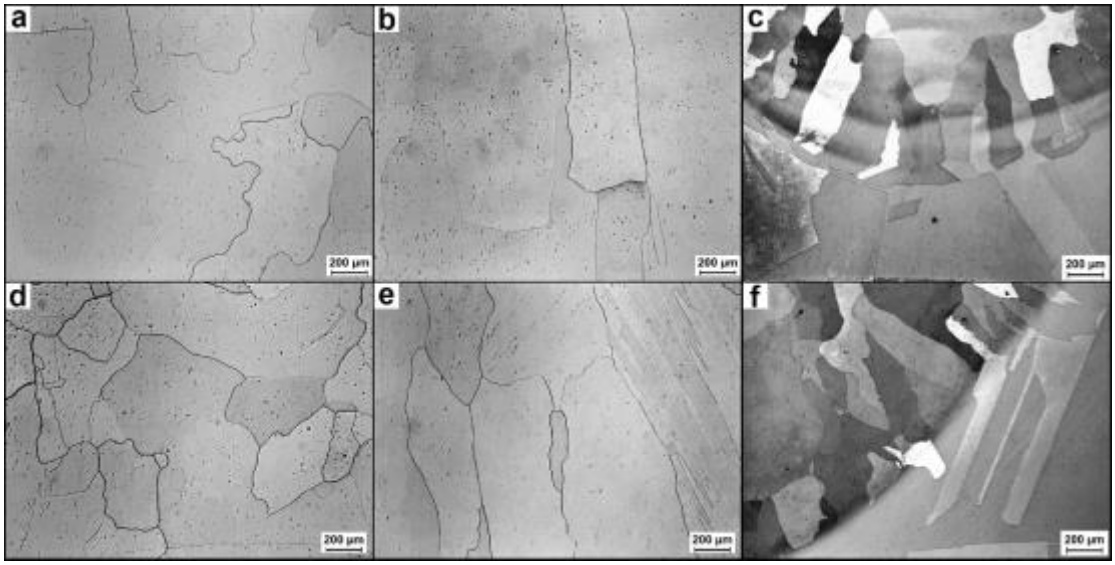

Figure 4. 3 Optical microstructures of Sample 2: (a) top section, (b) middle section, (c) bottom section; and Sample 3: (d) top section, (e) middle section, (f) bottom section

The microstructures of Sample 2 and Sample 3 from top, middle and bottom sections are shown in Fig.4.3. Compared with Sample 1, there is very clear grain refinement tendency in the microstructures of all three sections. The specific grain sizes measured according to ASTM E23 standard have been listed in Tab. 3. Besides the grain refinement, some unique lath-shaped structures are shown in the right-hand side of Fig.4.3 e, which is the middle section of Sample 3. These lath-shaped structures are the annealing twins induced by the grain refinement annealing. Since no such structure is found in Fig.4.3b, the middle section of Sample 2, it proves that the heat treatment temperature at 900 °C has the capability of changing the microstructure of columnar Cu-Al alloy. This phenomenon indicates that with enough heat treatment, the microstructures in Cu-Al alloys fabricated by WAAM process can be refined. In addition, the grain boundaries of both Sample 2 and Sample 3 are much more tortuous than Sample 1 in all sections, this is the consequence of crystal boundary migration induced by residual stress release during the homogenization annealing.

Table 3 The grain sizes of the three samples in top, middle and bottom section

	Top	Middle	Dilution
Sample 1	402 μm	949 μm	181 μm
Sample 2	312 μm	802 μm	144 μm
Sample 3	302 μm	755 μm	120 μm

Figure 4. 4 Microstructures near the top surface: (a) Sample 1; (b) Sample 2; (c) Sample 3

Microstructures near the top surface of three cross-section samples are shown in Fig. 4.4. The shear bands at the top of Sample 1 are induced by the grinding process. Theoretically, the shear bands should exist on each deposition layer. However, since the depth of the shear bands is very thin, it would be melted by the next layer of additive deposition process. Therefore, only the shear bands on the very top layer is observed in the entire buildup wall. In Fig.4.4 b and Fig.4.4 c, which are the microstructures near the top surface of Sample 2 and Sample 3, the shear bands have disappeared and

annealing twins are found in both photos, due to the homogenization annealing processes applied on the two samples. Compared with Sample 2, the annealing twins in Sample 3 are more complete and thorough since higher annealing temperature was applied. It can be seen that the annealing twins only exist on the very top surface rather than distributed in the entire sample. This is because the lattice structure of Cu-Al alloy is fcc structure, which has a strong inverse correlation of the twin density with the average grain size [94, 95]. As the columnar grains are much larger than the equiaxed grains, the twins can be barely found at other locations than the top surface.

4.2 Phase characterization

GBC® MMA X-ray diffractometer (XRD) with monochromatic Cu Kα radiation (=1.5418Å) was utilized to present phase characterization of Cu-Al annealed and non-annealed specimens. For the specific parameters, the scanning angle was set from 30 to 100 with 4 degree per minute and 0.02 step size. The voltage and loading current of the X-ray tube was 35kV and 28.6mA in this project.

The testing of XRD mainly follows the Bragg's law [96]:

$$n\lambda = 2d_{hkl} \sin \theta_{hkl}$$

in which λ is the wavelength of incident wave; *hkl* are the Miller indices of crystallographic planes of a crystalline phase; *d* is the interplanar spacing of specific *hkl* lattice planes; is the incident angle of the diffraction beam; and *n* is the order of reflection.

Figure 4. 5 GBC® MMA X-ray diffractometer (XRD) testing machine

4.2.1 Result and discussion

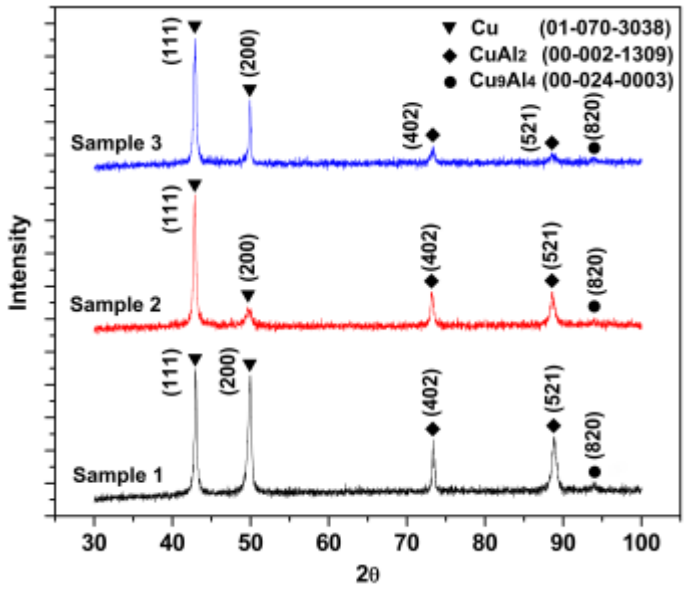

Figure 4. 6 XRD patterns of Sample 1, Sample 2 and Sample 3

The XRD spectrums of Sample 1, Sample 2 and Sample 3 are shown in Fig.4.6. In Sample 1, three phases have been detected by the diffraction including simple substance Cu (PDF No.: 01-070-3038) in (111) and (200) planes, Al_2Cu (PDF No.: 00-002-1309) in (402) and (521) planes, and Cu_9Al_4 (PDF No.: 00-024-1309) in (820) plane. As indicated by the intensity of peaks, the as-fabricated material mostly consists of Cu-Al solid solution and $CuAl_2$ with a small amount of Cu_9Al_4. According to the binary phase diagram, when Al content is lower than 16.8 at. %, both copper and aluminum should be α-phase (fcc structure). The existence of the two intermetallic phases is caused by the instability nature of welding process and lack of further homogenization. Since the rapid cooling rate of arc welding process (17-20.6 °C/s) [14], the aluminum liquid drop was solidified before diffusing into welding pool homogeneously. Thus, intermetallics, $CuAl_2$ and Cu_9Al_4, were generated. As shown in the spectrums of Sample 2 and Sample 3, after the homogenization annealing processes, both intermetallic Cu_9Al_4 and $CuAl_2$ experienced a significant decrease with the increase of annealing temperature. This phenomenon has also been observed during the Cu-Al alloy fabrication using powder metallurgy processes, in which the θ-$CuAl_2$ and γ-Cu_9Al_4 were firstly generated when Cu and 14 at. %Al are mixed; then with the further proceeding of ball-milling and homogenization, the $CuAl_2$ and Cu_9Al_4 transformed into Cu-Al solid solution alloy [81]. If insufficient energy is supplied during the fabricating process, $CuAl_2$ and Cu_9Al_4 would be produced in Cu-Al alloy even when the content of Al is lower than 2 at. %. [10]. In addition, oxides such as CuO and Al_2O_3, which have been detected during the ball milling process [9], are not detected in our XRD patterns. This indicates a good shielding protection during the present WAAM process.

Chapter 5 Composition and hardness

5.1 Measurement of aluminous composition

JEOL® JSM-6490LA scanning electron microscope (SEM) with OXFORD® X-Max^N energy disperse spectrometer (EDS) detector was used to measure the aluminium composition in Cu-Al welding sample. Three composition testing points were tested around the hardness testing point and the average of that was calculated. The error of composition measurement is approximately ±0.5 at.%. Additionally, in chapter 7, the metallographic photo of the surface of fractured tensile samples were also detected by this SEM machine.

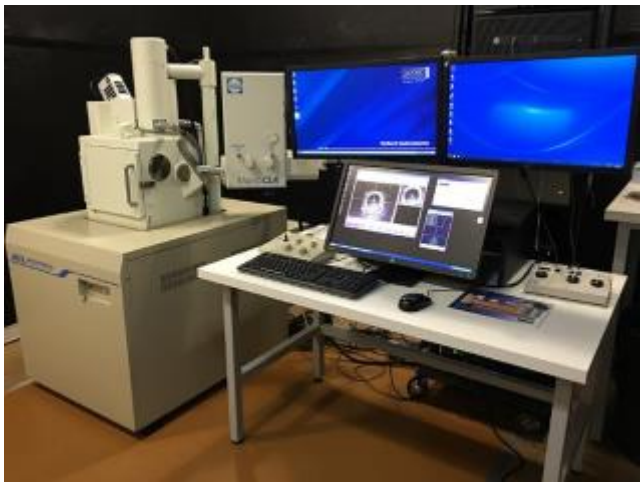

Figure 5. 1 JEOL® JSM-6490LA scanning electron microscope machine

5.2 Hardness testing

The hardness is a measure of how resistant solid matter is to various kinds of permanent shape change when a force is applied. It is one kind of intrinsic nature of material, which is mainly depended on the ductility, elastic stiffness, plasticity, strength and toughness. Because of the complex behavior of material under different type of force, the hardness measurements can be mainly divided into three types: scratch, indentation and rebound respectively. Indentation testing which is widely utilized in engineering and metallurgy fields was applied in present research. This method on the basic premise of measuring the critical dimensions of indentation pressed by a standard loaded indenter which is shown in Fig.5.2. The purpose of using indentation hardness measures is to measure the resistance of specimens about the material deformation caused by the constant compression load. Additionally, the result tested by indentation measurement can also correlate with the tensile testing.

Figure 5. 2 Pyramidal diamond anvil indenter [97]

Vickers's hardness test which was developed in 1922 by Smith and Sandland [98] is one of the typical indentation measurements. Compared with other methods, the Vickers's test is relatively easier since the results acquired by calculations are independent of the size of the indenter and the indenter is capable to all materials irrespective of the intrinsically mechanical properties. The hardness number, known as the Vickers pyramid number (HV), is calculated by the load over the surface area of the indentation and it can be converted into units of pascals. A diamond in the form of a square-based pyramid whose opposite sides meet at the apex at an angle of 136° serves as the intender [99]. While the intender is pressed into the surface of material, the angle between the surface of object and intender is 22° on each side (shown in Fig.5.3.).

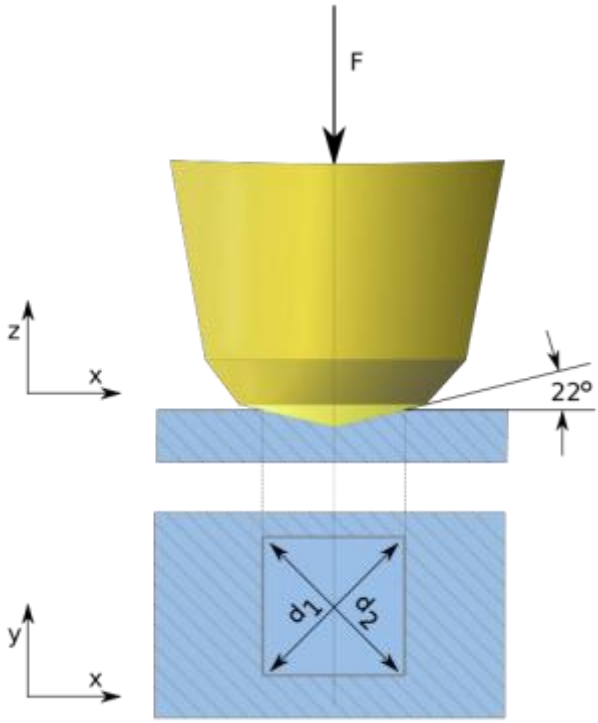

Figure 5. 3 Schematic of the theory of Vickers's hardness measurement [100]

Accordingly, the hardness number is calculated by the ratio of the force applied to the diamond in kilograms (F) and the surface area of the resulting indentation in square millimetres (A). Thus, the formulation of HV is presented below [101].

$$HV = \frac{F}{A} \approx \frac{1.8544F}{d^2}$$

the conversion is according to the following equation:

$$A = \frac{d^2}{2\sin{}^{136^\circ}/_{2}}$$

in which d represents the average length of the diagonal left by the indenter. In automatic hardness testing, the size of impression is measured by a calibrated

microscope.

In present study, Struers® DuraScan-70 automatic hardness indenter with 1kg loading was applied for the Vickers hardness test. The photograph of machine was shown in Fig.5.4. Additionally, the indentation time was set at 7 seconds in order to ensure the accuracy of hardness testing.

Figure 5. 4 Struers® DuraScan-70 automatic hardness indenter with 1kg loading

5.3 Result and discussion

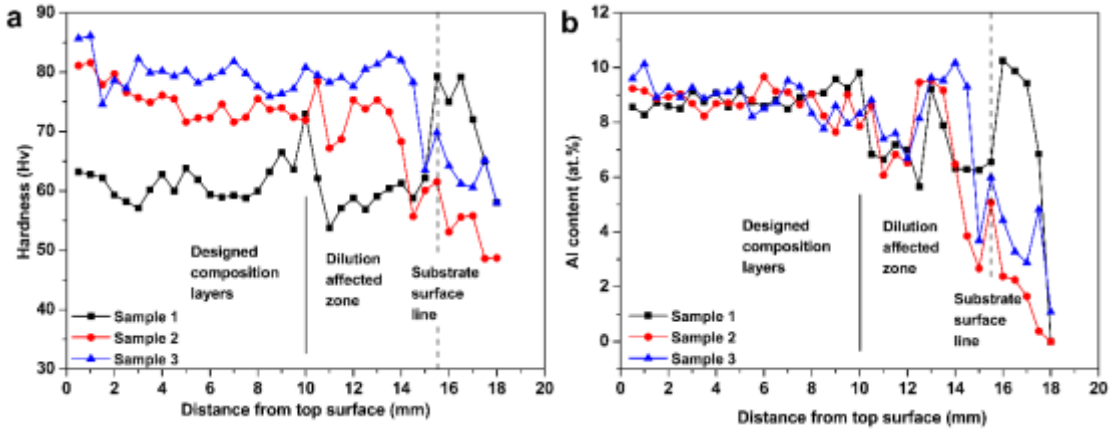

Figure 5. 5 (a) Hardness along the centerline of cross-section samples; (b) Al content near the hardness testing points

The hardness and Al content measurement of the cross-section samples as a function of the distance from top surface are shown in Fig.5.5. As shown in Fig.5.5b, the Al content in the dilution affected zone, from approximately 3 mm under the substrate surface to 5 mm above the surface, is significantly unstable, which leads to the fluctuation of hardness correspondingly as shown in Fig.5.5a. This is mainly due to the combination of two factors: (1) much slower feed speed of pure Al wire compared to Copper wire to achieve desired composition; (2) the extremely high thermal conductivity of the copper substrate make it difficult for the tungsten torch to open the molten pool with adequate size in the first few layers. Both of two negative influences lead to large discontinuous Al droplet from the Al wire transforming into the molten pool. Therefore, the deposited liquid phase Cu would have already transformed into solid phase before the Cu and Al can be homogeneously mixed by the molten pool and the Al content of Sample 1 has a non-uniform distribution at the dilution effected zone.

However, at middle and top region, the molten pool is generated on the Cu-Al mixture, which is more inclined to absorb Al material and has relatively lower thermal conductivity. Therefore, the chemical composition and hardness curves turn out to be relatively homogeneous after a few layers above the dilution affected zone. In addition, as presented in the previous research, during the WAAM process, a few previous layers will be remelted during the current layer of deposition, which also provides a chance to homogenize the chemical composition in the neighboring layers [11]. As a result, for the regions above the dilution effected zone, the Al content of the three samples are much more homogeneous and have a mean value of 8.9 at. %, which is very close to the designed value of 9 at. %.

The average hardness of the three samples experiences an increasing trend with the increase of heat-treatment temperature, with 61.7 Hv, 75.1 Hv and 79.5 Hv respectively for Sample 1, Sample 2 and Sample 3. The improvement of hardness is due to the solid solution strengthening effect and the grains were also refined, as the detected intermetallics $CuAl_2$ and Cu_9Al_4 transformed into Cu-Al solid solution during the annealing process. Furthermore, above the dilution affected zone, both heat treated specimens exhibit slightly higher hardness value at the top region due to smaller grain size at the top of the sample. There should be even higher hardness in the area of annealing twins near the top surface. However, in order to ensure the entire hardness indentation located inside of the cross-section sample, the hardness tests were applied from 0.5 mm under the very top surface. For the as-fabricated sample, however, the fluctuation of hardness due to the inhomogeneity make the trend less obvious.

In addition, as shown in Fig. 5.5, higher Al content in the buildup Cu-Al alloy has led to higher hardness in the corresponding locations. This is due to the solution strengthening effect and the existence of $CuAl_2$ and Cu_9Al_4 intermetallic phases, which possess higher hardness because of their intermetallic nature [102, 103]. The hardness of Cu-Al alloy fabricated by WAAM process is lower than those obtained from the reference work, in which the hardness and strength of Cu-Al solid solution are higher than copper. This is mainly due to the lack of further mechanical processing (such as rolling and pressing) to generate desired twin structure, which lead to material strengthening.

Overall, Sample 3 showed better and more homogenized material properties. Therefore, the homogenization annealing method of Sample 3 has been chosen to further process the additive manufactured Cu-Al alloy for the tensile test.

Chapter 6 Tensile test

Tensile testing is one of the technique to measure the mechanical properties. Normally, the sample for tensile testing is subjected to a controlled tension until failure. In practice, the result of tensile testing is mainly utilized to select a material for application and to predict how a material will be influenced by the forces. In tension testing, ultimate tensile strength, elongation and yield strength can be exhibited. In this respect, the strain (ε) of material can be calculated via the elongation, using the following equation [104]:

$$\varepsilon = \frac{\Delta L}{L_0} = \frac{L - L_0}{L_0}$$

in which L_0 is the original gauge length and L is the finial length. At the same time, the stress (σ) can also be calculated according to the formulate [105]:

$$\sigma = \frac{F_n}{A}$$

where F_n represents the tensile force while A represents nominal cross-section of the specimen. According to these two data, the strain-stress curve can be graphed.

In present study, the gauge volume for the tensile sample is 10mm×2mm×1.5mm. MTS370 load unit at $5\times10^{-3}s^{-1}$ strain rate was used for tensile testing at the room temperature. In addition, SEM image of the facture surface were present to analyse the fracture principle.

Figure 6. 1 MTS370 tensile testing machine

6.1 Result and discussion

The room temperature ultimate tensile strength (UTS), 0.2% offset yield strength (0.2%YS) and the elongation of as-fabricated sample and the sample annealed at 900 °C for 2 hours are summarized in Tab. 3. It can be observed that the UTS and 0.2% YS have experienced a slight increase after the heat treatment, from 231 MPa to 241 MPa

and from 63 MPa to 67 MPa respectively. In addition, the elongation has increased 13% from 63% in the as-fabricated sample to 76% in the annealed sample. The improvements of UTS and 0.2%YS are mainly due to the grain refinement and further solid solution effect happened during the annealing.

As Al has the property of decreasing the stacking fault energy in solid solutions [106], the improvement of elongation is partially contributed by the increase of twinning activity due to the decline of stacking fault energy. During plastic deformation, material with low stacking fault energy is more inclined to produce twin and twinning mechanism can also support further deformation, which leads to the improvement of elongation [87]. The similar result was also reported in previous work that twin improves the strength and ductility simultaneously during tensile testing [107].

Table 4 Tensile test results of samples under as-fabricated and 900 ℃ for 2 h

	UTS (MPa)	0.2% YS (MPa)	Elongation (%)
As-fabricated	231 ±2.5	63 ±2.1	63 ±4.0
900 °C for 2 h	241 ±3.1	67 ±2.0	76 ±6.7

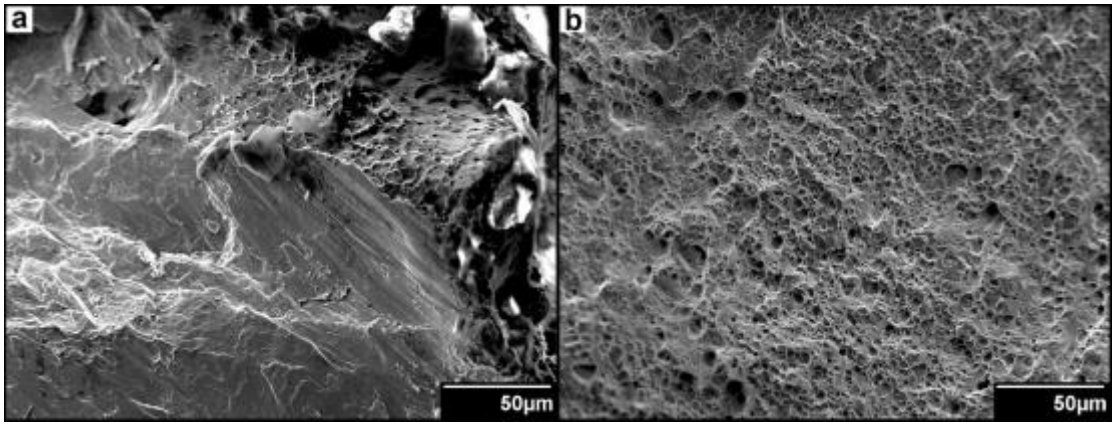

Figure 6. 2 SEM micrographs of fractures: (a) as-fabricated; (b) 900 ℃ for 2 h

The fracture surfaces of the as-fabricated and annealed samples are shown in Fig.6.2. Typical ductile fractures have been found in the surfaces. This is as expected since the elongations of the samples are very high. The fracture surface of the as-fabricated specimens mainly consists of shear dimples with a few equiaxed dimples near the edge of the fracture, while in the annealed sample only equiaxed dimples exist. These characteristics have in another way proved that the homogenization annealing has improved the ductility of the Cu-Al alloy. Therefore, for the Cu-Al alloy fabricated by WAAM process, homogenization annealing process is necessary for obtaining the more homogenized structure and better material properties.

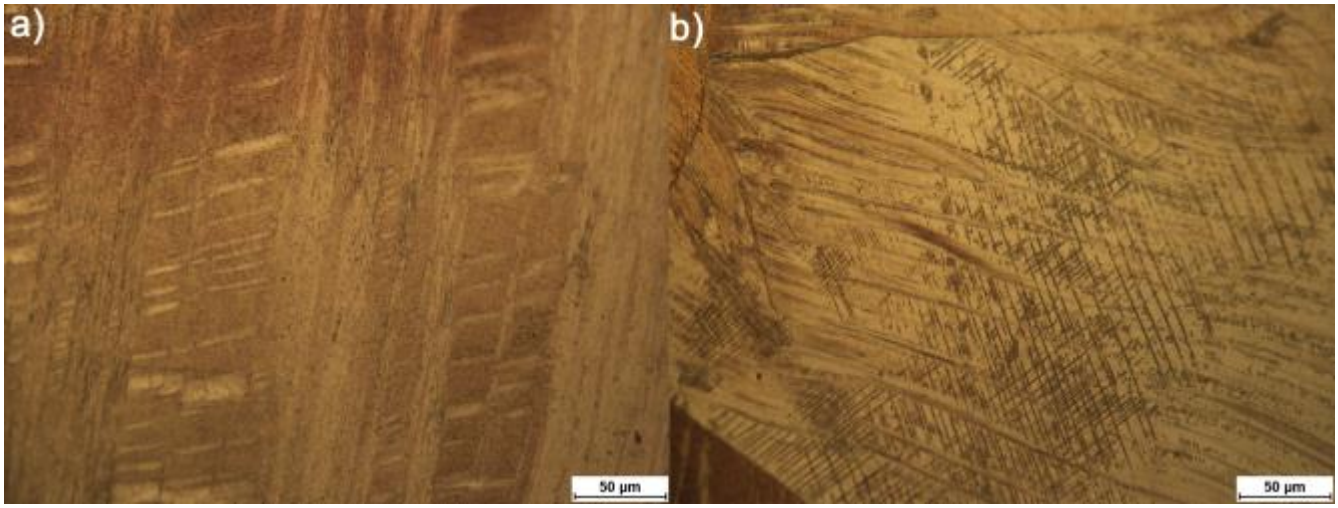

Figure 6. 3 Optical microstructures of tensile samples: a) as-fabricated sample; b) 900 ℃ for 2 h

The optical microstructures of as-fabricated and annealed at 900°C samples after tensile testing at the room temperature are presented in Fig.6.3. Shear bands with parallel strips are observed in the as-fabricated sample as shown in Fig.6.3 (a), while the shear bands in the annealed sample are step-shaped and disordered, which can be seen in Fig.6.3 (b). Normally, shear bands are developed after the sever plastic deformation (tensile test is one type of plastic deformation) for the ductile material as it mainly caused by intense shearing strain. Thus, the higher density of shear bands in the annealing sample proves that sample annealed at 900°C possesses higher ductility than the as-fabricated one. It is consistent with the elongation calculated by S-S curve.

Furthermore, a wide range of polycrystalline alloys deform through shear caused by shear bands. To some extent, these phenomena show the anisotropy of material at the grain scale, which is corresponding to the microstructures of Cu-Al buildup wall. In addition, in 2016, Wei et. al reported the microstructure and tensile properties of Cu-Al

solid solution with different SFE [108]. They also found shear bands developed after equal channel angular pressing (ECAP) and cryoECAP. It was indicated that the shear bands generated via post work in Cu-Al alloy are clusters of deformation twin by TEM observation. With the lower of SFE, the density of twins in shear bands is higher. Thus, according to the optical microstructure, the present study speculates that the density twin in annealing sample is higher than the as-fabricated one because of higher content of Cu-Al solid solution in annealing sample.

Chapter 7 Conclusion and future work

The final chapter mainly presents a general conclusion of this thesis and provides recommendations of the potential future work related to Wire-Arc Additive Manufacturing (WAAM) systems according to the review of current stage and outcome of present subject.

7.1 Conclusion

This thesis presents the feasibility study of in-situ producing Cu-Al alloy using twin wire WAAM process. The present research has opened a gate of in-situ fabrication of Cu-Al alloy with target chemical composition and full-density using additive manufacturing process. In order to obtain better and more homogenized material properties, homogenization annealing processes were applied to the as-fabricated deposit. Afterwards, the microstructure, phase characterization and mechanical properties were tested and reported.

A general conclusion of the results acquired from the present study is listed below:

Initially, referring to the conventional welding process and the properties of copper and aluminum, the setup including the software and hardware of WAAM system was completed. In terms of the specific parameters, the deposition current was 160A and the arc length was 3.5 mm, to ensure sufficient local heat input for opening the molten pool on the pure copper substrate; the wire-feed speeds of Cu and Al wires were 1300 mm/min and 311 mm/min, respectively; the average deposition energy was controlled at

20.2 kJ/g in order to ensure the deposition stability and the travel speed was set at 95 mm/min; in order to open the molten pool on the copper plate, the interpass temperature was set at 400°C. Additionally, to prevent the copper substrate from being penetrated and deformed by the high-energy torch, the substrate was fixed on a 5 mm DH36 steel plate. The appropriate setup guaranteed the 15-layer Cu-Al wall fabricated successfully.

Subsequently, considering the high cooling rate of welding process, this thesis compared as-fabricated and annealed buildup wall via investigating their microstructure and phase characterization. In terms of the microstructure, all samples exhibited large columnar grains in the middle region, while the relatively equiaxed grains were detected in the top region. However, the grain size of annealed sample was relatively lower than the counterpart of as-fabricated sample, which illustrated the refinement function of annealing process. Moreover, it is interesting to note that annealing twin crystal was observed at the very top region of annealed sample. The deformation of twin crystal was due to the low SFE of Cu-Al. Phase characterization of three types of specimens was investigated. It showed that after the homogenization annealing processes, the impurity phases Cu_9Al_4 and $CuAl_2$ were reduced with the increasing annealing temperature.

Furthermore, according to the measurement, for the regions above the dilution effected zone, the Al content of the three samples are much more homogeneous and had a mean value of 8.9 at. %, which was very close to the designed value of 9 at. %. It to some extent verified the feasibility of WAAM to fabricated Cu-Al with stable composition. On the other hand, the average hardness of the three samples experienced an increasing trend with the increase of heat-treatment temperature, with 61.7 Hv, 75.1 Hv and 79.5 Hv respectively. It was caused by the solid solution strength.

In addition, the room temperature ultimate tensile strength (UTS), 0.2% offset yield strength (0.2%YS) and the elongation as-fabricated sample and the sample annealed at 900 °C for 2 hours were summarized. It could be observed that the UTS and 0.2% YS have experienced a slight increase after the heat treatment, from 231 MPa to 241 MPa and from 63 MPa to 67 MPa respectively. In addition, the elongation has increased 13% from 63% in the as-fabricated sample to 76% in the annealed sample.

Generally, the WAAM process has proved its capability of in-situ producing Cu-Al binary alloy with pre-designed chemical composition. Under as-fabricated condition, intermetallic phases such as $CuAl_2$ and Cu_9Al_4 were detected in the deposit. After homogenization annealing processes, contents of the intermetallics were decreased with the increase of annealing temperature. Also, the mechanical properties of the Cu-Al alloy, hardness, ultimate tensile strength, yield strength and elongation, were increased by the homogenization annealing processes. And with higher annealing temperature, the improvements of mechanical properties were more obvious.

7.2 Future work

The present research has made progress in successfully applying the Wire-Arc Additive Manufacturing (WAAM) process for in-situ fabricating the copper-rich Cu-Al alloy with designed composition. However, further understanding of Cu-Al binary alloy and development of WAAM system are desired in the future work. Thus, the recommendations were summarized below according to the present study.

The further post fabrication processes such as cold works to refine the grain size of buildup Cu-Al component is desired. As presented in the experimental results, the grain inside the Cu-Al based buildup components are all extremely large columnar grains, although the grains were refined via deformation annealing twin crystal in the very top region. The large grain size leads to the weak hardness of sample. With low SFE, Cu-Al solid solution is capable to generate deformation twin which can acquire nano-level crystal. On such occasion, the hardness and tensile strength can be increased extremely.

The study on the samples after tensile test is also another research direction. Tensile testing is one kind of plastic deformation and deformation twin can be obtained after tensile test. Thus, hardness test can be utilized again for the tensile samples to compare transformation of mechanical properties. In addition, TEM and EBSD method can be used for analyzing the texture and preferred direction of twin crystal in order to understand the theory of generating deformation twin.

Moreover, temperature gradient can be extended as well as the time in annealing process. For instance, the time of annealing process can be increased to 8h even 16h, while the annealing temperature can be set at 950°C or 1000°C. In this respect, more appropriate annealing process can be acquired through comparing the various group samples.

In terms of the WAAM process, further development for the current parameters is needed. As shown in the present research, further development of the WAAM process in specific areas such as interpass temperature control, gas shielding and integrating the twin wire WAAM process to welding robots is desired for the application in modern

industry.

References

[1] L. M. Dimaté Castellanos, J. J. Olaya Flórez, A. Orjuela, and J. Edgar, "Corrosion resistance of Cu-Al coatings produced by thermal spray," *Ingeniería e Investigación,* vol. 32, pp. 18-23, 2012.

[2] A. Rohatgi, K. S. Vecchio, and G. T. Gray III, "The influence of stacking fault energy on the mechanical behavior of Cu and Cu-Al alloys: Deformation twinning, work hardening, and dynamic recovery," *Metallurgical and Materials Transactions A,* vol. 32, pp. 135-145, 2001.

[3] J. Tao, K. Yang, H. Xiong, X. Wu, X. Zhu, and C. Wen, "The defect structures and mechanical properties of Cu and Cu–Al alloys processed by split Hopkinson pressure bar," *Materials Science and Engineering: A,* vol. 580, pp. 406-409, 2013.

[4] V. Rajkovic, D. Bozic, J. Stasic, H. Wang, and M. T. Jovanovic, "Processing, characterization and properties of copper-based composites strengthened by low amount of alumina particles," *Powder Technology,* vol. 268, pp. 392-400, 2014.

[5] X. Liu, I. Ohnuma, R. Kainuma, and K. Ishida, "Phase equilibria in the Cu-rich portion of the Cu–Al binary system," *Journal of alloys and compounds,* vol. 264, pp. 201-208, 1998.

[6] M. Lebienvenu, G. Ocampo, and B. Dubois, "Internal friction, tensile tests and hardness variations during the tempering of an as-quenched Cu-10wt.% Al alloy," *Materials Science and Engineering,* vol. 47, pp. 77-88, 1981.

[7] B. Ahuja, L. M. Kang, K. Y. Nagulin, and M. Schmidt, “Fabrication and characterization of high strength Al-Cu alloys processed using laser beam melting in metal poweder bed,” *Physics Procedia*, vol. 56, pp.135-146,

[8] O. Johari and G. Thomas, "Substructures in explosively deformed Cu and Cu-Al alloys," *Acta Metallurgica,* vol. 12, pp. 1153-1159, 1964.

[9] D. V. Dudina, O. I. Lomovsky, K. R. Valeev, S. F. Tikhov, N. N. Boldyreva, A. N. Salanov*, et al.*, "Phase evolution during early stages of mechanical alloying of Cu–13wt.% Al powder mixtures in a high-energy ball mill," *Journal of Alloys and Compounds,* vol. 629, pp. 343-350, 2015.

[10] H. Wang, R. Zhang, X. Hu, C.-A. Wang, and Y. Huang, "Characterization of a powder metallurgy SiC/Cu–Al composite," *journal of materials processing technology,* vol. 197, pp. 43-48, 2008.

[11] C. Shen, Z. Pan, Y. Ma, D. Cuiuri, and H. Li, "Fabrication of iron-rich Fe–Al intermetallics using the wire-arc additive manufacturing process," *Additive Manufacturing,* vol. 7, pp. 20-26, 2015.

[12] D. Ding, Z. Pan, D. Cuiuri, and H. Li, "Wire-feed additive manufacturing of metal components: technologies, developments and future interests," *The International Journal of Advanced Manufacturing Technology,* vol. 81, pp. 465-481, 2015.

[13] M. J. Bermingham, D. Kent, H. Zhan, D. H. StJohn, and M. S. Dargusch, "Controlling the microstructure and properties of wire arc additive manufactured Ti–6Al–4V with trace boron additions," *Acta Materialia,* vol. 91, pp. 289-303, 2015.

[14] H. T. Lee and J. L. Wu, "The effects of peak temperature and cooling rate on the susceptibility to intergranular corrosion of alloy 690 by laser beam and gas tungsten arc welding," *Corrosion Science,* vol. 51, pp. 439-445, 2009.

[15] Y. Zhang and S. Zhang, "Welding aluminum alloy 6061 with the opposing dual-torch GTAW process," *WELDING JOURNAL-NEW YORK-,* vol. 78, pp. 202-s, 1999.

[16] Y. Ma, D. Cuiuri, N. Hoye, H. Li, and Z. Pan, "The effect of location on the microstructure and mechanical properties of titanium aluminides produced by

additive layer manufacturing using in-situ alloying and gas tungsten arc welding," *Materials Science and Engineering: A,* vol. 631, pp. 230-240, 2015.

[17] C. Shen, Z. Pan, D. Cuiuri, B. Dong, and H. Li, "In-depth study of the mechanical properties for Fe 3 Al based iron aluminide fabricated using the wire-arc additive manufacturing process," *Materials Science and Engineering: A,* vol. 669, pp. 118-126, 2016.

[18] Y. Ma, D. Cuiuri, N. Hoye, H. Li, and Z. Pan, "Effects of wire feed conditions on in situ alloying and additive layer manufacturing of titanium aluminides using gas tungsten arc welding," *Journal of Materials Research,* vol. 29, pp. 2066-2071, 2014.

[19] C. Shen, Z. Pan, D. Cuiuri, J. Roberts, and H. Li, "Fabrication of Fe-FeAl Functionally Graded Material Using the Wire-Arc Additive Manufacturing Process," *Metallurgical and Materials Transactions B,* vol. 47, pp. 763-772, 2016.

[20] H. Huang, M. Nie, Y. Luan, X. Liu, and J. Xie, "Fatigue property of single-crystal and columnar-grained polycrystalline Cu-12wt.% Al Alloys," *Procedia Engineering,* vol. 27, pp. 1686-1693, 2012.

[21] Y. Wang, H.-Y. Huang, and J.-X. Xie, "Enhanced room-temperature tensile ductility of columnar-grained polycrystalline Cu–12wt.% Al alloy through texture control by Ohno continuous casting process," *Materials Letters,* vol. 65, pp. 1123-1126, 2011.

[22] L. Kloc, J. Fiala, and J. Čadek, "Creep in a Cu-14at.% Al solid solution alloy at intermediate temperatures and low stresses," *Materials Science and Engineering: A,* vol. 130, pp. 165-172, 1990.

[23] S. I. Hong and C. Laird, "Cyclic-hardening behavior of polycrystalline Cu-16at.% Al alloy," *Materials Science and Engineering: A,* vol. 142, pp. 1-9, 1991.

[24] M. Yamashita, M. Yoshioka, T. Mimaki, S. Hashimoto, and S. Miura, "Stress-corrosion-cracking of (100)-twist boundaries in Cu-9at.% Al alloy," *Acta Metallurgica et Materialia,* vol. 38, pp. 1619-1623, 1990.

[25] C. Engelke, J. Plessing, and H. Neuhäuser, "Plastic deformation of single glide oriented Cu-2 to 15at.% Al crystals at elevated temperatures," *Materials Science and Engineering: A,* vol. 164, pp. 235-239, 1993.

[26] Y. Tian, C. Hang, C. Wang, and Y. Zhou, "Evolution of Cu/Al intermetallic compounds in the copper bump bonds during aging process," in *Electronic Packaging Technology, 2007. ICEPT 2007. 8th International Conference on*, 2007, pp. 1-5.

[27] K. V. Wong and A. Hernandez, "A review of additive manufacturing," *ISRN Mechanical Engineering,* vol. 2012, 2012.

[28] S. Ashley, "Rapid prototyping is coming of age," *Mechanical Engineering,* vol. 117, p. 62, 1995.

[29] K. Cooper, *Rapid prototyping technology: selection and application*: CRC press, 2001.

[30] T. Wohlers and T. Gornet, "History of additive manufacturing," *Wohlers Report: Additive Manufacturing and 3D Printing State of the Industry Annual Worldwide Progress Report,* 2011.

[31] J.-P. Kruth, "Material incress manufacturing by rapid prototyping techniques," *CIRP Annals-Manufacturing Technology,* vol. 40, pp. 603-614, 1991.

[32] T. T. Wohlers, *Wohlers report 2009: State of the industry annual worldwide progress report*: Wohlers Associates, 2009.

[33] G. N. Levy, R. Schindel, and J.-P. Kruth, "Rapid manufacturing and rapid tooling with layer manufacturing (LM) technologies, state of the art and future

perspectives," *CIRP Annals-Manufacturing Technology,* vol. 52, pp. 589-609, 2003.

[34] S. Singh, S. Ramakrishna, and R. Singh, "Material issues in additive manufacturing: A review," *Journal of Manufacturing Processes,* vol. 25, pp. 185-200, 2017.

[35] M. A. Jackson, A. Van Asten, J. D. Morrow, S. Min, and F. E. Pfefferkorn, "A Comparison of Energy Consumption in Wire-based and Powder-based Additive-subtractive Manufacturing," *Procedia Manufacturing,* vol. 5, pp. 989-1005, 2016.

[36] I. A. Roberts, C. J. Wang, M. Stanford, K. A. Kibble, and D. J. Mynors, "Experimental and Numerical Analysis of Residual Stresses in Additive Layer Manufacturing by Laser Melting of Metal Powders," in *Key Engineering Materials*, 2011, pp. 461-465.

[37] M. Seifi, A. Salem, J. Beuth, O. Harrysson, and J. J. Lewandowski, "Overview of materials qualification needs for metal additive manufacturing," *JoM,* vol. 68, pp. 747-764, 2016.

[38] L. V. Antony and R. G. Reddy, "Processes for production of high-purity metal powders," *JOM,* vol. 55, p. 14, 2003.

[39] E. A. Nasr, A. Al-Ahmari, A. Kamrani, and K. Moiduddin, "Digital design and fabrication of customized mandible implant," in *World Automation Congress (WAC), 2014*, 2014, pp. 1-6.

[40] P. Heinl, L. Müller, C. Körner, R. F. Singer, and F. A. Müller, "Cellular Ti–6Al–4V structures with interconnected macro porosity for bone implants fabricated by selective electron beam melting," *Acta biomaterialia,* vol. 4, pp. 1536-1544, 2008.

[41] Y. Liu, S. Li, W. Hou, S. Wang, Y. Hao, R. Yang*, et al.*, "Electron beam melted beta-type Ti–24Nb–4Zr–8Sn porous structures with high strength-to-modulus

ratio," *Journal of Materials Science & Technology,* vol. 32, pp. 505-508, 2016.

[42] V. Petrovic, J. Vicente Haro Gonzalez, O. Jorda Ferrando, J. Delgado Gordillo, J. Ramon Blasco Puchades, and L. Portoles Grinan, "Additive layered manufacturing: sectors of industrial application shown through case studies," *International Journal of Production Research,* vol. 49, pp. 1061-1079, 2011.

[43] B. Ralph, "Method of making decorative articles," ed: Google Patents, 1925.

[44] S. Williams, F. Martina, A. Addison, J. Ding, G. Pardal, and P. Colegrove, "Wire þ Arc Additive Manufacturing."

[45] P. Kazanas, P. Deherkar, P. Almeida, H. Lockett, and S. Williams, "Fabrication of geometrical features using wire and arc additive manufacture," *Proceedings of the Institution of Mechanical Engineers, Part B: Journal of Engineering Manufacture,* vol. 226, pp. 1042-1051, 2012.

[46] Y. Ma, D. Cuiuri, N. Hoye, H. Li, and Z. Pan, "Characterization of in-situ alloyed and additively manufactured titanium aluminides," *Metallurgical and Materials Transactions B,* vol. 45, pp. 2299-2303, 2014.

[47] V. Fahimpour, S. Sadrnezhaad, and F. Karimzadeh, "Microstructure and mechanical property change during FSW and GTAW of Al6061 alloy," *Metallurgical and Materials Transactions A,* vol. 44, pp. 2187-2195, 2013.

[48] K. Moore, D. Naidu, R. Yender, and J. Tyler, "Gas metal arc welding control: Part I: Modeling and analysis," *Nonlinear Analysis: Theory, Methods & Applications,* vol. 30, pp. 3101-3111, 1997.

[49] J. Ding, P. Colegrove, J. Mehnen, S. Ganguly, P. S. Almeida, F. Wang*, et al.*, "Thermo-mechanical analysis of wire and arc additive layer manufacturing process on large multi-layer parts," *Computational Materials Science,* vol. 50, pp. 3315-3322, 2011.

[50] R. P. Reis, D. Souza, and D. Ferreira Filho, "Arc interruptions in Tandem pulsed gas metal arc welding," *Journal of Manufacturing Science and Engineering,* vol. 137, p. 011004, 2015.

[51] C. Shen, "Low distortion welding for shipbuilding industry," 2013.

[52] J. Nadzam, "Tandem GMAW Offers Quality Weld Deposits, High Travel Speeds," *Welding Design and Fabrication,* vol. 76, pp. 28-31, 2003.

[53] V. Fersini and S. Matera, "The synchronized tandem wire welding process applied to the welding of structural plates," *Welding International,* vol. 23, pp. 597-605, 2009.

[54] T. Ueyama, T. Ohnawa, K. Yamazaki, M. Tanaka, M. Ushio, and K. Nakata, "High-Speed Welding of Steel Sheets by the Tandem Pulsed Gas Metal Arc Welding Systemt," *Transactions of the JWRI,* vol. 34, pp. 11-18, 2005.

[55] F. Martina, J. Mehnen, S. W. Williams, P. Colegrove, and F. Wang, "Investigation of the benefits of plasma deposition for the additive layer manufacture of Ti–6Al–4V," *Journal of Materials Processing Technology,* vol. 212, pp. 1377-1386, 2012.

[56] W. J. Zhang, Y. K. Liu, and Y. M. Zhang, *Real-Time Measurement of Three Dimensional Weld Pool Surface in GTAW*: INTECH Open Access Publisher, 2012.

[57] A. T. Zimmer and P. Biswas, "Characterization of the aerosols resulting from arc welding processes," *Journal of Aerosol Science,* vol. 32, pp. 993-1008, 2001.

[58] C. Weisman, *Welding handbook*: American Welding Society, 1976.

[59] N. Lv, Y. Xu, J. Zhong, H. Chen, J. Wang, and S. Chen, "Research on detection of welding penetration state during robotic GTAW process based on audible arc sound," *Industrial Robot: An International Journal,* vol. 40, pp. 474-493, 2013.

[60] S. Richard, "The procedure handbook of arc welding," *The Lincoln Electric Company, Cleveland, Ohio,* pp. 5.41-5.49, 1995.

[61] H. Wang, W. Jiang, J. Ouyang, and R. Kovacevic, "Rapid prototyping of 4043 Al-alloy parts by VP-GTAW," *Journal of Materials Processing Technology,* vol. 148, pp. 93-102, 2004.

[62] F. Bonaccorso, L. Cantelli, and G. Muscato, "Arc welding Control for Shaped Metal Deposition Process," *IFAC Proceedings Volumes,* vol. 44, pp. 11636-11641, 2011.

[63] S. Hongyuan, H. Xixia, L. Tao, and C. Shanben, "Weld formation control for arc welding robot," *The International Journal of Advanced Manufacturing Technology,* vol. 44, pp. 512-519, 2009.

[64] C. J. Bloch, D. Harrison, and J. Hill, "Apparatus and method for computerized interactive control, measurement and documentation of arc welding," ed: Google Patents, 1998.

[65] S. Kou, "Welding metallurgy," *New York,* 1987.

[66] K. Moore, M. Abdelrahman, and D. Naidu, "Gas metal arc welding control–II. Control strategy," *Nonlinear Analysis: Theory, Methods & Applications,* vol. 35, pp. 85-93, 1999.

[67] V. Subravel, G. Padmanaban, and V. Balasubramanian, "Effect of welding speed on microstructural characteristics and tensile properties of GTA welded AZ31B magnesium alloy," *Transactions of Nonferrous Metals Society of China,* vol. 24, pp. 2776-2784, 2014.

[68] C. De Facci and P. C. Duerr, "Welding gas shield control," ed: Google Patents, 1981.

[69] P. Wongpanya, T. Böllinghaus, G. Lothongkum, and T. Kannengießer, "Effects of preheating and interpass temperature on stresses in S 1100 QL multi-pass butt-welds," *Welding in the World,* vol. 52, pp. 79-92, 2008.

[70] A. Moarrefzadeh and M. Sadeghi, "Numerical simulation of copper temperature field in gas tungsten arc welding (GTAW) process," in *Proceedings of the 10th WSEAS international conference on Robotics, control and manufacturing technology*, 2010, pp. 26-31.

[71] J. R. Pedersen, D. M. Parker, and R. G. Trechel, "Copper alloy welding filler and method of use," ed: Google Patents, 1984.

[72] C. Fan, F. Lv, and S. Chen, "Visual sensing and penetration control in aluminum alloy pulsed GTA welding," *The International Journal of Advanced Manufacturing Technology,* vol. 42, pp. 126-137, 2009.

[73] G. L. Hira, T. A. Osial, and W. A. Ernst, "Method of welding aluminum alloys," ed: Google Patents, 1987.

[74] M. Li and S. Zinkle, "4.20-Physical and Mechanical Properties of Copper and Copper Alloys," *Compr. Nucl. Mater., Elsevier, Oxford,* pp. 667-690, 2012.

[75] N. Stojanovic, D. Maithripala, J. Berg, and M. Holtz, "Thermal conductivity in metallic nanostructures at high temperature: Electrons, phonons, and the Wiedemann-Franz law," *Physical Review B,* vol. 82, p. 075418, 2010.

[76] A. Griffin, S. Hernandez, F. Brotzen, and C. Dunn, "A Galvanic Series for Thin-Film Metallizations and Barrier Layers Commonly Used in the Microelectronics Industry," *Journal of The Electrochemical Society,* vol. 141, pp. 807-809, 1994.

[77] A. Atrens, J. Nairn, H. Fernee, K. FitzGerald, G. Skennerton, and A. Olofinjana, "Copper alloys," in *Materials Forum*, 1997, pp. 57-78.

[78] A. Nadkarni, E. Ling, and P. Taubenblat, "High conductivity copper and aluminum alloys," *Ling, E., Taubenblat, PW, Eds,* p. 77, 1984.

[79] L. Lu, Y. Shen, X. Chen, L. Qian, and K. Lu, "Ultrahigh strength and high electrical conductivity in copper," *Science,* vol. 304, pp. 422-426, 2004.

[80] X. An, Q. Lin, S. Wu, and Z. Zhang, "Microstructural evolution and shear fracture of Cu–16at.% Al alloy induced by equal channel angular pressing," *Materials Science and Engineering: A,* vol. 527, pp. 4510-4514, 2010.

[81] D. Ying and D. Zhang, "Solid-state reactions between Cu and Al during mechanical alloying and heat treatment," *Journal of Alloys and Compounds,* vol. 311, pp. 275-282, 2000.

[82] I.-W. Chen, "Migration assisted diffusional creep by grain-boundary diffusion," *Acta Metallurgica,* vol. 30, pp. 1317-1323, 1982.

[83] H. Jiang, J. Dai, H. Tong, B. Ding, Q. Song, and Z. Hu, "Interfacial reactions on annealing Cu/Al multilayer thin films," *Journal of applied physics,* vol. 74, pp. 6165-6169, 1993.

[84] M. Shearer, C. Bauer, and A. Jordan, "Investigation of interdiffusion in thin film couples of aluminum and copper by Auger electron spectroscopy," *Thin Solid Films,* vol. 61, pp. 273-279, 1979.

[85] L. Dubourg, H. Pelletier, D. Vaissiere, F. Hlawka, and A. Cornet, "Mechanical characterisation of laser surface alloyed aluminium–copper systems," *Wear,* vol. 253, pp. 1077-1085, 2002.

[86] D. R. Steinmetz, T. Jäpel, B. Wietbrock, P. Eisenlohr, I. Gutierrez-Urrutia, A. Saeed–Akbari*, et al.*, "Revealing the strain-hardening behavior of twinning-induced plasticity steels: Theory, simulations, experiments," *Acta Materialia,* vol. 61, pp. 494-510, 2013.

[87] J. Tao, G. Chen, W. Jian, J. Wang, Y. Zhu, X. Zhu*, et al.*, "Anneal hardening of a nanostructured Cu–Al alloy processed by high-pressure torsion and rolling," *Materials Science and Engineering: A,* vol. 628, pp. 207-215, 2015.

[88] R. Fullman and J. Fisher, "Formation of annealing twins during grain growth,"

Journal of Applied Physics, vol. 22, pp. 1350-1355, 1951.

[89] J. Cahoon, Q. Li, and N. Richards, "Microstructural and processing factors influencing the formation of annealing twins," *Materials science and engineering: a,* vol. 526, pp. 56-61, 2009.

[90] D. Field, R. Eames, and T. Lillo, "The role of shear stress in the formation of annealing twin boundaries in copper," *Scripta materialia,* vol. 54, pp. 983-986, 2006.

[91] S. Qu, X. An, H. Yang, C. Huang, G. Yang, Q. Zang*, et al.*, "Microstructural evolution and mechanical properties of Cu–Al alloys subjected to equal channel angular pressing," *Acta Materialia,* vol. 57, pp. 1586-1601, 2009.

[92] F. Montevecchi, G. Venturini, A. Scippa, and G. Campatelli, "Finite Element Modelling of Wire-arc-additive-manufacturing Process," *Procedia CIRP,* vol. 55, pp. 109-114, 2016.

[93] F. Wang, S. Williams, and M. Rush, "Morphology investigation on direct current pulsed gas tungsten arc welded additive layer manufactured Ti6Al4V alloy," *The international journal of advanced manufacturing technology,* vol. 57, pp. 597-603, 2011.

[94] Y. Jin, M. Bernacki, A. Agnoli, B. Lin, G. S. Rohrer, A. D. Rollett*, et al.*, "Evolution of the annealing twin density during δ-supersolvus grain growth in the nickel-based superalloy Inconel™ 718," *Metals,* vol. 6, p. 5, 2015.

[95] G. Wang, H. Peng, C. Zhang, S. Wang, and Y. Wen, "Relationship among grain size, annealing twins and shape memory effect in Fe–Mn–Si based shape memory alloys," *Smart Materials and Structures,* vol. 25, p. 075013, 2016.

[96] P. A. Heiney, "1.3-Bragg's Law," 2016.

[97] R. Smith and G. Sandly, "An accurate method of determining the hardness of

metals, with particular reference to those of a high degree of hardness," *Proceedings of the Institution of Mechanical Engineers,* vol. 102, pp. 623-641, 1922.

[98] E. S. George and L. S. Robert, "Apparatus for testing the hardness of materials," ed: Google Patents, 1923.

[99] G. Farges and D. Degout, "Interpretation of the indentation size effect in vickers microhardness measurements-absolute hardness of materials," *Thin Solid Films,* vol. 181, pp. 365-374, 1989.

[100] V. B. DO AMARAL, "Ultralow Friction System: Liquid Crystals onto Boron Nitride/Diamond-Like Carbon Multilayered Films Deposited by Plasma Enhanced Chemical Vapor Deposition," *wear,* vol. 12, p. 16.

[101] P. J. Blau, *Microindentation techniques in materials science and engineering: a symposium sponsored by ASTM Committee E-4 on Metallography and by the International Metallographic Society, Philadelphia, PA, 15-18 July 1984*: Astm International, 1986.

[102] A. T. Adorno and R. A. G. Silva, "Ageing behavior in the Cu–10wt.%Al and Cu–10wt.%Al–4wt.%Ag alloys," *Journal of Alloys and Compounds,* vol. 473, pp. 139-144, 2009.

[103] H. H. Kuo, W. H. Wang, and Y. F. Hsu, "Microstructural characterization of precipitates in Cu–10wt.%Al–0.8wt.%Be shape-memory alloy," *Materials Science and Engineering: A,* vol. 430, pp. 292-300, 2006.

[104] J. R. Davis, *Tensile testing*: ASM international, 2004.

[105] V. Tvergaard, A. Needleman, and K. K. Lo, "Flow localization in the plane strain tensile test," *Journal of the Mechanics and Physics of Solids,* vol. 29, pp. 115-142, 1981.

[106] M. Denanot and J. Villain, "The stacking fault energy in Cu-Al-Zn alloys," *physica status solidi (a),* vol. 8, pp. K125-K127, 1971.

[107] R. Kumar, S. Dasharath, P. Kang, C. C. Koch, and S. Mula, "Enhancement of mechanical properties of low stacking fault energy brass processed by cryorolling followed by short-annealing," *Materials & Design,* vol. 67, pp. 637-643, 2015.

[108] W. Wei, S. L. Wang, K. X. Wei, I. V. Alexandrov, Q. B. Du, and J. Hu, "Microstructure and tensile properties of Cu Al alloys processed by ECAP and rolling at cryogenic temperature," *Journal of Alloys and Compounds,* vol. 678, pp. 506-510, 2016.